

The Miller Range 090340 and 090206 meteorites: Identification of new brachinite-like achondrites with implications for the diversity and petrogenesis of the brachinite clan

Cyrena Anne GOODRICH^{1,2,*}, Noriko T. KITA³, Stephen R. SUTTON^{4,5}, Sue WIRICK⁵, and Juliane GROSS^{6,7}

¹Lunar and Planetary Institute, 3600 Bay Area Blvd, Houston, Texas 77058, USA

²Planetary Science Institute, 1700 E. Ft. Lowell Drive, Tucson, Arizona 85719, USA

³Wisc-SIMS, University of Wisconsin, Madison, Wisconsin 53706, USA

⁴Department of Geophysical Sciences, University of Chicago, Chicago, Illinois 60637, USA

⁵Center for Advanced Radiation Sources, University of Chicago, Chicago, Illinois 60637, USA

⁶Department of Earth and Planetary Sciences, Rutgers University, 610 Taylor Rd, Piscataway, New Jersey 08854, USA

⁷Department of Earth and Planetary Sciences, The American Museum of Natural History, New York, New York 10024, USA

*Corresponding author. E-mail: goodrich@lpi.usra.edu

(Received 28 October 2015; revision accepted 12 January 2017)

Abstract—Miller Range (MIL) 090340 and MIL 090206 are olivine-rich achondrites originally classified as ureilites. We investigate their petrography, mineral compositions, olivine Cr valences, equilibration temperatures, and (for MIL 090340) oxygen isotope compositions, and compare them with ureilites and other olivine-rich achondrites. We conclude that they are brachinite-like achondrites that provide new insights into the petrogenesis of brachinite clan meteorites. MIL 090340,6 has a granoblastic texture and consists of ~97 modal % by area olivine (Fo = molar Mg/[Mg+Fe] = 71.3 ± 0.6). It also contains minor to trace augite, chromite, chlorapatite, orthopyroxene, metal, troilite, and terrestrial Fe-oxides. Approximately 80% by area of MIL 090206,5 has a granoblastic texture of olivine (Fo 72.3 ± 0.1) plus minor augite and chromite, similar to MIL 090340 but also containing minor plagioclase. The rest of the section consists of a single crystal of orthopyroxene (~11 × 3 mm), poikilitically enclosing rounded grains of olivine (Fo = 76.1 ± 0.6), augite, chromite, metal, and sulfide. Equilibration temperatures for MIL 090340 and MIL 090206, calculated from olivine-spinel, olivine-augite, and two-pyroxene thermometry range from ~800 to 930 °C. In both samples, symplectic intergrowths of Ca-poor orthopyroxene + opaque phases (Fe-oxides, sulfide, metal) occur as rims on and veins/patches within olivine. Before terrestrial weathering, the opaques were probably mostly sulfide, with minor metal. All petrologic properties of MIL 090340 and MIL 090206 are consistent with those of brachinite clan meteorites, and largely distinct from those of ureilites. Oxygen isotope compositions of olivine in MIL 090340 ($\delta^{18}\text{O} = 5.08 \pm 0.30\text{‰}$, $\delta^{17}\text{O} = 2.44 \pm 0.21\text{‰}$, and $\Delta^{17}\text{O} = -0.20 \pm 0.12\text{‰}$) are also within the range of brachinite clan meteorites, and well distinguished from ureilites. Olivine Cr valences in MIL 090340 and the granoblastic area of MIL 090206 are 2.57 ± 0.06 and 2.59 ± 0.07 , respectively, similar to those of three brachinites also analyzed here (Brachina, Hughes 026, Nova 003). They are higher than those of olivine in ureilites, even those containing chromite. The valence systematics of MIL 090340, MIL 090206, and the three analyzed brachinites (lower Fo = more oxidized Cr) are consistent with previous evidence that brachinite-like parent bodies were inherently more oxidized than the ureilite parent body. The symplectic orthopyroxene + sulfide/metal assemblages in MIL 090340, MIL 090206, and many brachinite clan meteorites have superficial similarities to characteristic “reduction rims” in ureilites. However, they differ significantly in detail. They likely formed by reaction of olivine with S-rich fluids, with only minor reduction. MIL 090340 and the granoblastic area

of MIL 090206 are similar in modal mineralogy and texture to most brachinites, but have higher Fo values typical of brachinite-like achondrites. The poikilitic pyroxene area of MIL 090206 is more typical of brachinite-like achondrites. The majority of their properties suggest that MIL 090340 and MIL 090206 are residues of low-degree partial melting. The poikilitic area of MIL 090206 could be a result of limited melt migration, with trapping and recrystallization of a small volume of melt in the residual matrix. These two samples are so similar in mineral compositions, Cr valence, and cosmic ray exposure ages that they could be derived from the same lithologic unit on a common parent body.

INTRODUCTION

The Miller Range (MIL) 090340 olivine-rich achondrite, and paired sample MIL 090356, were originally classified as ureilites (AMN 34, #1, 2011) and reported to have olivine compositions of Fo (= molar Mg/[Fe+Mg]) 70–73, which is more ferroan than olivine in known ureilites (~75–95). The MIL 090206 olivine-rich achondrite was classified as a ureilite with olivine of Fo 72–74 (AMN 34, #2, 2011), and also reported to contain a significant amount of orthopyroxene, which is uncommon in ferroan ureilites. We began an investigation of MIL 090340 and MIL 090206 because they could potentially extend the range of known ureilite properties and provide new information about ureilite petrogenesis. Warren and Rubin (2012) began an investigation of MIL 090340 and MIL 090356 for similar reasons. They concluded that this meteorite is not a ureilite and suggested instead a kinship with brachinites. A subsequently described similar meteorite, MIL 090963, was classified as an ungrouped achondrite (AMN 35, #1, 2012). Goodrich et al. (2012) reported oxygen isotope data showing MIL 090340 to be within the range of brachinites. The six similar meteorites MIL 090340, MIL 090356, MIL 090206, MIL 090895, MIL 090963, and MIL 090405 were subsequently reclassified as ungrouped achondrites “possibly related to brachinites” (AMN 35, #2, 2012). Corder et al. (2014) also concluded that MIL 090206 and MIL 090405 were linked to brachinites based on oxygen isotope data.

This study details and augments the work of Goodrich et al. (2012), presenting a study of the petrography, mineral compositions, valences of Cr in olivine, oxygen isotope compositions, and equilibration temperatures of MIL 090340 and MIL 090206. We compare these properties of MIL 090340 and MIL 090206 with those of ureilites, brachinites and brachinite-like achondrites, and other olivine-rich asteroidal meteorites. The primary goal of this comparison is to determine whether MIL 090340 and MIL 090206 are related to any previously known meteorites, i.e., how they should be classified. A further goal is to investigate grain boundary assemblages of orthopyroxene + opaques

that occur in MIL 090340 and MIL 090206. These assemblages superficially resemble the characteristic “reduction rims” of ureilites (Mittlefehldt et al. 1998), and probably account for the original classification of MIL 090340 and MIL 090206 as ureilites, as in the case of brachinite-like achondrite NWA 1500 (Goodrich et al. 2011). We investigate these assemblages in detail, compare them with reduction rims in ureilites, and discuss possible mechanisms for their origin. We also discuss other aspects of MIL 090340 and MIL 090206 that offer new insights into the petrogenesis of brachinites and brachinite-like achondrites.

As background to the comparisons and discussion in this study, we give brief summaries of the properties of ureilites and brachinite clan meteorites, the two achondrite groups to which MIL 090340 and MIL 090206 have previously been suggested to belong.

Brief Summary of Properties of Ureilites

Main group ureilites (currently >375 individual meteorites) are carbon-rich ultramafic achondrites (see reviews in Mittlefehldt et al. 1998; Goodrich et al. 2004; Krot et al. 2013). They are composed of olivine and pyroxene (pyroxene abundance from ~10 to 70 modal %), with ≤ 10 modal % interstitial graphite (\pm diamond), metal, and sulfides. They are medium to coarse grained (~0.1 to several mm-sized) with equilibrated textures (rounded grain boundaries with common triple junctions), and commonly display a fabric defined by both a lineation and a foliation. Olivine and pyroxene core compositions are very homogenous within each sample, with olivine composition varying from Fo ~75 to 95 among samples. In the majority of main group ureilites, the sole pyroxene is pigeonite (Wo 5–13). Orthopyroxene (Wo ≤ 5) occurs in addition to, or instead of, pigeonite in ureilites of Fo ~87 to 92. A small subgroup of main group ureilites (~4–5% of all ureilite samples) contains augite as a major phase. One of the characteristic features of ureilites is the presence of “reduction rims” on olivine grains. These consist of Mg-enriched olivine containing numerous $\leq \mu\text{m}$ -sized grains of metal

(Wlotzka 1972). Ureilites are distinguished from all other achondrites by their oxygen isotope compositions, which span a large range of $\Delta^{17}\text{O}$ values (-0.5 to -2.5‰) and are nearly coincident with the CCAM (carbonaceous chondrite anhydrous mineral; Clayton and Mayeda 1999) array on a 3-oxygen isotope plot.

Brief Summary of Properties of Brachinites and Brachinite-Like Achondrites (the Brachinite Clan)

Brachinites are olivine-rich achondrites with up to 15 modal % augite; various abundances of plagioclase (0–10 modal %); and minor to trace abundances of orthopyroxene, chromite, phosphates, metal, and sulfides (see reviews by Keil [2014] and Krot et al. [2013]). Their olivine-rich areas have medium to coarse grained (0.1 to 1.5 mm-sized) granoblastic textures with curved grain boundaries and triple junctions, while augite and plagioclase grains commonly show intergranular morphologies. Preferred orientation and foliation have been reported in two brachinites (Warren and Kallemeyn 1989; Mittlefehldt et al. 2003). Silicate compositions are homogeneous within most brachinite samples, with olivine compositions ranging from Fo 64 to 68.

Brachinite-like olivine-rich achondrites were defined by Day et al. (2012) as having many characteristics similar to those of brachinites, but containing significantly more orthopyroxene and having more magnesian olivine and pyroxene compositions (e.g., Fo 70–80). We note also that the pyroxenes in brachinite-like achondrites commonly have poikilitic textures, which are rare in brachinites. However, there are many inconsistencies in the literature over the classification of some meteorites as brachinites, brachinite-like achondrites, or ungrouped achondrites. In this study, we compare MIL 090340 and MIL 090206 with 26 meteorites that have been classified as brachinites or suggested to have affinities to brachinites. We consider fourteen of these samples (or their pairing groups) to be brachinites, eight to be brachinite-like, and another four that have some similarities to brachinites (Divnoe, Tafassasset, Zag(b) and LEW 88763) to be ungrouped. This classification does not completely agree with that of Day et al. (2012), who include Divnoe and Zag(b) with brachinite-like achondrites. There are also twelve meteorites that are currently classified as brachinites in the Meteoritical Bulletin Database but have not yet been studied in detail and are not considered in this work. See Table S1 in supporting information for a list of these 38 meteorites.

The oxygen isotope compositions of brachinites and brachinite-like achondrites are similar to those of the HED meteorites, but show a greater range of $\Delta^{17}\text{O}$ values, from ~ 0 to 0.4‰ . Several recent papers have

compiled tables of properties of brachinites and brachinite-like achondrites (Mittlefehldt et al. 2003; Goodrich et al. 2011; Day et al. 2012; Gardner-Vandy et al. 2013; Keil 2014).

SAMPLES AND METHODS

Optical and Electron Microscopy and Electron Microprobe Analyses

We studied thin sections MIL 090340,6 and MIL 090206,5. Optical and electron microscopy was performed in the Department of Geosciences at the University of Massachusetts, Amherst (U. Mass) and the American Museum of Natural History, New York (AMNH). Backscattered electron (BEI) imaging was performed using the Zeiss EVO50-XVP scanning electron microscope (SEM) at U. Mass. Electron microprobe analyses (EMPA) and wavelength-dispersive (WDS) X-ray mapping were performed using the Cameca SX-50 electron microprobe at U. Mass and the Cameca SX-100 electron microprobe at AMNH. All analyses utilized natural and synthetic minerals, glasses, oxides, and/or metals as standards. Silicate minerals were analyzed using 15 KeV and 30–60 nA beam current. Olivine cores were analyzed at 60 nA, with 100–400 second peak counting times for MnO, Cr_2O_3 , Al_2O_3 , and CaO, and 40 second peak counting times for MgO, FeO, and SiO_2 . Olivine cores in the Kenna ureilite were analyzed during every olivine probe run to ensure consistency with previous olivine data of Goodrich et al. (1987, 2001, 2006, 2014). Phosphates and plagioclase were analyzed at 10 nA with 10–20 second counting times and a defocused (nominally 2 μm diameter) beam. Pyroxenes and chromites were analyzed at 30 nA with 10–60 second peak counting times. V_2O_3 abundances in chromites were corrected for overlap of the Ti $\text{K}\beta$ peak with the V $\text{K}\alpha$ peak. To ensure the accuracy of this correction, two different procedures were tested. Details are given in Table S2 in supporting information. Sulfides and metals were analyzed using 15 KeV and 40–50 nA beam current.

Modal abundances were determined by manual point counting of whole-section collages of BEI (MIL 090340,6: 1147 points, $\sim 115 \text{ mm}^2$) or combined Mg-Ca-Al X-ray maps (MIL 090206,5: 3647 points, $\sim 148 \text{ mm}^2$), after identification of all major phases by EDS and EMPA.

Oxygen Isotope Analyses by Secondary Ion Mass Spectrometry (SIMS)

Oxygen three isotopes of olivine in thin section MIL 090340,6 were analyzed using a secondary ion mass spectrometer IMS 1280 at WiseSIMS laboratory.

The analytical conditions are similar to those reported in Kita et al. (2010) and Goodrich et al. (2011) using multicollector Faraday cups. The primary ion beam was set to 15 μm diameter with an intensity of ~ 3.5 nA and the secondary ^{16}O ion intensities were $(4\text{--}5) \times 10^9$ cps for olivine. San Carlos (SC) olivine standard (Fo_{89}) and another olivine standard (Fo_{60}) were used to estimate the instrumental bias correction for olivine in MIL 090340 (Table S3 in supporting information). The reproducibility of repeated analyses of SC olivine was $\leq 0.2\%$ for $\delta^{18}\text{O}$ and $\leq 0.4\%$ for $\delta^{17}\text{O}$ and $\Delta^{17}\text{O}$. Locations of analysis positions for unknown olivine were restricted to within 5 mm from the center of the SIMS sample holder in order to avoid possible analytical artifacts near the edge of the sample holder (Kita et al. 2009). Final results of unknown data include propagated uncertainties of instrumental bias across a SIMS mount, which are 0.3% and 0.15% for $\delta^{18}\text{O}$ and $\delta^{17}\text{O}$, respectively (Kita et al. 2009, 2010). The effect of ^{16}OH interference to ^{17}O signal was much smaller than 0.1% and thus insignificant.

The deviation of oxygen isotope ratios from the terrestrial fractionation line for MIL 090340 was calculated as $\Delta^{17}\text{O}$ using the equation $\Delta^{17}\text{O} = \delta^{17}\text{O} - 0.52 \times \delta^{18}\text{O}$ (e.g., Clayton and Mayeda 1999). The $\delta^{18}\text{O}$ values of mineral standards were calibrated to the VSMOW-scale using laser fluorination analyses (e.g., Kita et al. 2010), but $\delta^{17}\text{O}$ values are assumed to obey the same linear mass fractionation law. Compared to the power law by Miller (2002) with a coefficient of $\lambda = 0.5247$ as in Greenwood et al. (2012), our $\Delta^{17}\text{O}$ values are systematically lower by 0.02% at $\delta^{18}\text{O}$ values of 5% . However, since $\Delta^{17}\text{O}$ values of unknowns are estimated relative to the San Carlos olivine standard, the calculated $\Delta^{17}\text{O}$ values are almost identical using the two methods as long as $\delta^{18}\text{O}$ values of the unknowns are similar to San Carlos olivine.

X-Ray Absorption Near Edge Structure (XANES) Analyses

We used X-ray Absorption Near Edge Structure (XANES) to measure Cr valence in olivines in thin sections MIL 090340 (section,6) and MIL 090206 (section,5), as well as brachinites Brachina (AMNH4489-1), Hughes 026 (AMNH4883-2) and Nova 003 (AMNH4815-2), and ureilites HaH 064 (University of Münster), Shisr 007 (courtesy of R. Bartoschewitz), LAP 02382 (section,5), and META78008 (section,49). Locations of analyses in the MIL sample thin sections are shown in Figs. S1 and S2 in supporting information. The XANES spectra were collected at the X26A beamline at the National Synchrotron Light Source (NSLS) located at Brookhaven National Laboratory, Upton, NY, USA

(Sutton et al. 2002). The NSLS was a second-generation synchrotron source which ran at 2.8 GeV in non-top-off-mode. The X26A beamline was located on a hard bend magnet with a maximum photon flux at 10 keV of 10^{12} ph/sec/0.1% BW/mrad. The monochromator consisted of silicon (111) and (311) channel cut crystals which were both available for use and the (111) crystal was used in this study. The beam was focused onto the samples with a spot size of ~ 7 microns using Rh-coated Kirkpatrick-Baez mirrors. Some spectra were also collected using the X-ray microprobe at Beamline 13-ID-E (GSECARS) at the Advanced Photon Source (APS), Argonne, IL. A Si (111) monochromator was also used there, with a KB mirror focal spot of ~ 1 μm . For each instrument, the monochromator energy was calibrated using the XANES spectrum from a 5 μm thick Cr foil where the energy of the first derivative peak was defined to be 5989 eV.

Chromium XANES spectra were collected using the following range sets: 5960–5985 eV with 5 eV step size and a dwell time of 5 s; 5985.2–6020 eV with step size of 0.2 eV and dwell time of 5 s; 6020.2–6200 eV with a step size of 2 eV and a dwell time of 5 s with each spectrum taking 45 minutes to collect. A SII NanoTechnology USA, Inc. ME4 silicon drift detector (SDD) was used on both instruments (the NSLS instrument also used two SII single channel SDDs for a total of six detectors) which were used to collect Cr K fluorescence photons. Spectra collected from standards of glasses containing Cr^{2+} and Cr^{3+} were used to determine valence states for the samples (Goodrich et al. 2013a) expressed as values between 2.0 and 3.0.

The synchrotron X-ray beams are linearly polarized and therefore XANES spectra for anisotropic crystals vary slightly with crystal orientation. To at least partially correct for these effects, spectra were collected at four different orthogonal orientations of the thin sections (-0° , 90° , 180° , 270°) for all samples. Cr XANES spectra were collected on 8 and 19 olivine grains for MIL 090340 and MIL 090206, respectively. All of the olivine valence state data were obtained by first merging the spectra for each olivine grain at the four different orientation angles with reference to the x-ray beam. The program ATHENA (Ravel and Newville 2005) was used to determine Cr valence states and its use is described in detail by Goodrich et al. (2013a). To summarize, the absorption peak at 5994 eV represents a $1s \rightarrow 4s$ transition with orbital mixing. Measuring the derivative peak intensity of this absorption and comparing this peak intensity to the peak intensities of the Cr^{2+} and Cr^{3+} standards result in a valence state for the area analyzed. The ratio $\text{Cr}^{2+}/\text{Cr}^{3+}$ is calculated as $(3 - \text{Cr valence})/(\text{Cr valence} - 2)$.

Using the Cr valence results, oxygen fugacity estimates were obtained using the approach of

Goodrich et al. (2013a), based on the experimental work on basalts by Hanson and Jones (1998). We used their equation for the dependence of $\text{Cr}^{2+}/\text{Cr}^{3+}$ in a basaltic melt on $f\text{O}_2$ at 1200 °C:

$$\log(\text{Cr}^{2+}/\text{Cr}^{3+}) = 0.241 * (-\log f\text{O}_2) - 2.47 \quad (1)$$

The oxygen fugacity relative to the iron-wüstite buffer (ΔIW) at 1200 °C was derived from:

$$\Delta\text{IW} = \log f\text{O}_2 - (-11.94) \quad (2)$$

We assume, based on discussion in Goodrich et al. (2013a), that the partitioning between olivine and melt (D) is 1.0 for both Cr^{2+} and Cr^{3+} (i.e., olivine has no preference for divalent or trivalent Cr). These values may be affected by melt composition, as parameterized by NBO/T (Hanson and Jones 1998). The use of Equation 1 assumes a basaltic composition, but the compositional effects are small. Using the entire range of reasonable NBO/T values (0.2–1.2 for rhyolitic to ultramafic), $D(\text{Cr}^{3+})$ varies only from 0.85 to 1.25, while $D(\text{Cr}^{2+})$ is invariant with NBO/T (Hanson and Jones 1998), leading to a total potential error in $f\text{O}_2$ smaller than our quoted typical $f\text{O}_2$ uncertainty of ± 0.5 log units (see Goodrich et al. 2013a). Possible errors due to lower equilibration temperature are discussed in the paper.

RESULTS

General Petrography

MIL 090340,6 is an olivine-dominated rock with protogranular to granoblastic texture (Figs. 1a and 1b). Modal mineral abundances by area are ~97% olivine, ~0.6% chromite, ~0.5% augite, $\leq 1\%$ opaques (Fe-sulfide; Fe,Ni metal; and Fe-oxides and/or -hydroxides), with trace amounts of phosphate and orthopyroxene. Olivine grain sizes range from ~50 to 800 μm , with most grains being ~300–350 μm . The studied section contains one grain of augite, ~800 μm in maximum dimension, which has an intergranular morphology and partially poikilitically encloses surrounding olivine grains (Fig. 2a). We found no primary orthopyroxene, although Warren and Rubin (2012) reported it as a rare phase in another section of this meteorite. Large chromite grains (of which there are four in the section) are anhedral and range from ~0.5 to 1.6 mm in maximum dimension (Fig. 3a). They commonly have narrow rims and/or crosscutting veins of Fe-oxides/hydroxides, assumed to be terrestrial weathering products (Fig. 3a). Chromite also occurs as a few highly rounded (nearly circular in section) grains ~10–40 μm in

diameter, completely enclosed in olivine (Fig. 3b). The one observed phosphate grain is a highly rounded (nearly circular in section) grain ~35 μm in diameter, and is completely enclosed in olivine with a partial rim of tiny (unidentified) opaque grains (Fig. 2c).

Fine-grained intergrowths of orthopyroxene + opaque mineral grains (Fe-sulfide, Fe-oxides/hydroxides, rare metal) occur as linings/rims along almost all olivine grain margins, and also as crosscutting veins and patches within olivine grains (Fig. 1b). These intergrowths are described in more detail below. Sulfide and rare metal also occur as larger (~20–150 μm) anhedral grains along grain boundaries (e.g., Fig. 3e). One subhedral metal grain (~60 μm) occurs as an inclusion in a large chromite grain (Fig. 3a). Fe-oxides/hydroxides, assumed to be terrestrial weathering products, are pervasive along grain boundaries and common as veins and patches within mineral grains.

MIL 090206,5 has overall modal abundances (by area) of ~75% olivine, 16% orthopyroxene, 2% augite, 2% chromite, 1% plagioclase, and 4% opaques (Fe-sulfide, metal and Fe-oxides and/or-hydroxides). Orthopyroxene occurs mainly in one ~11 \times 3 mm-sized area, comprising a single crystal that poikilitically encloses rounded grains of chromite, olivine, rare augite, sulfide, and metal (Fig. 4). The nonpoikilitic area of the section is olivine-dominated with a protogranular to granoblastic texture (Figs. 1c and 1d). Olivine grain sizes range from ~100 μm to 1 mm, with most grains being 300–600 μm . Most chromite occurs as large anhedral to intergranular/poikilitic grains ranging from ~350 μm to 1.4 mm in size (Figs. 3c and 3d). These grains commonly have rims and/or crosscutting veins and patches of Fe-oxides/hydroxides, assumed to be terrestrial weathering products (Figs. 3c and 3d). One chromite grain is a small, nearly circular grain ~40 μm in diameter, completely enclosed in olivine. Augite occurs as anhedral to intergranular poikilitic grains, ~50 to 730 μm in size (Fig. 2b). Plagioclase occurs as anhedral masses with intergranular and poikilitic (enclosing olivine grains) morphology, concentrated in one ~2.3 \times 4.5 mm-sized area of the section (Figs. 2d and 4a). Olivine, augite, and chromite chadocrysts in the poikilitic area (Fig. 4b) are all smaller than their counterparts in the nonpoikilitic area.

Fine-grained intergrowths of orthopyroxene + opaque mineral grains (Fe-sulfide, Fe-oxides/hydroxides, rare metal) occur as linings/rims along almost all olivine grain margins, and also as crosscutting veins and patches within olivine (Figs. 1d, 2b, and 2d). These intergrowths are described in more detail below. Sulfide and metal also occur as isolated larger (up to ~150 μm) anhedral grains along grain

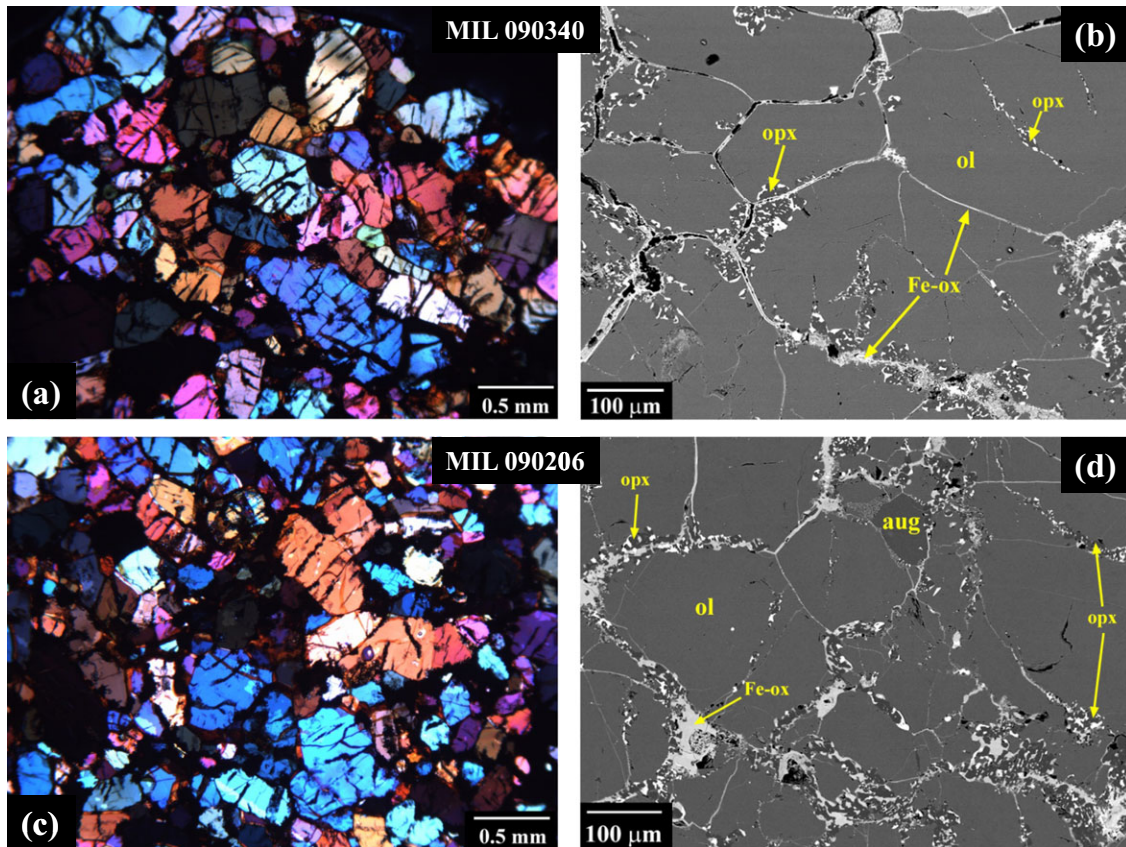


Fig. 1. Images showing general textures of MIL 090340,6 and MIL 090206,5 (nonpoikilitic area). Transmitted crossed-polarized light in (a) and (c). Backscattered electron images (BEI) in (b) and (d). Both meteorites consist largely of olivine (ol) grains, with minor augite (aug). A characteristic feature is that the margins of all olivine grains are lined with fine-grained intergrowths of orthopyroxene (opx) plus opaques (bright grains in BEI). Fe-oxides (Fe-ox), presumably terrestrial, are common along all grain boundaries.

boundaries (Fig. 3f) and within the orthopyroxene oikocryst. They appear to be better preserved (less affected by terrestrial weathering) within and around the margins of the oikocryst. Fe-oxides/hydroxides, assumed to be terrestrial weathering products, are pervasive along grain boundaries and common as veins and patches within mineral grains.

Mineral Compositions

MIL 090340

Compositions of olivine in MIL 090340 range from Fo 70 to 73, with an average value of Fo 71.3 ± 0.6 (Table 1, Fig. 5a). These values are similar to the range Fo 71.5 to 73.4 reported for a different section of MIL 090340 by Warren and Rubin (2012). Most grains show no significant zonation, but a few were found to be reverse zoned, with slightly higher Fo (by ~ 0.5 – 1.5 Fo units) near grain boundaries or adjacent to internal veins of orthopyroxene+opaques (Fig. 5b). Minor element contents in olivine are 0.08 ± 0.1 wt% CaO

and 0.04 ± 0.1 wt% Cr_2O_3 , with molar Fe/Mn = 54.0 ± 1.7 (Table 1, Fig. 6). Augite is Wo (= molar Ca/[Ca+Mg+Fe]) 42.6 ± 1 , mg# (= molar Mg/[Mg+Fe]) 81.6 ± 0.8 , with ~ 0.7 wt% Al_2O_3 , 0.75 wt% Cr_2O_3 , and 0.45 wt% Na_2O (Table 2, Fig. 7). Orthopyroxene in grain boundary intergrowths is Wo ~ 0.9 , mg# 78, with ~ 0.1 wt% Cr_2O_3 , and TiO_2 , Al_2O_3 and Na_2O contents near or below detection limits (Table 2). For comparison, the primary orthopyroxene reported by Warren and Rubin (2012) in another section of this meteorite was Wo 3.3, mg# 74.1.

Compositions of large chromite grains are nearly uniform at fe# (= molar $\text{Fe}^{2+}/[\text{Fe}^{2+}+\text{Mg}]$) ~ 76 – 77 and Cr# (= molar Cr/[Cr+Al]) ~ 84.4 , with ~ 2.4 wt% TiO_2 and 0.73 wt% V_2O_3 (Table 3; Figs. 8 and 9). They show slight normal zonation, with outermost rims having fe# up to 1.3 units higher than grain interiors (Fig. 8). The small round chromite grains (e.g., Fig. 3b) are unzoned. They have Cr# and TiO_2 contents similar to those of the large chromites, but are more ferroan with fe# ~ 84 – 85 , and have slightly lower V_2O_3 of ~ 0.65 – 0.7 wt% (Table 3).

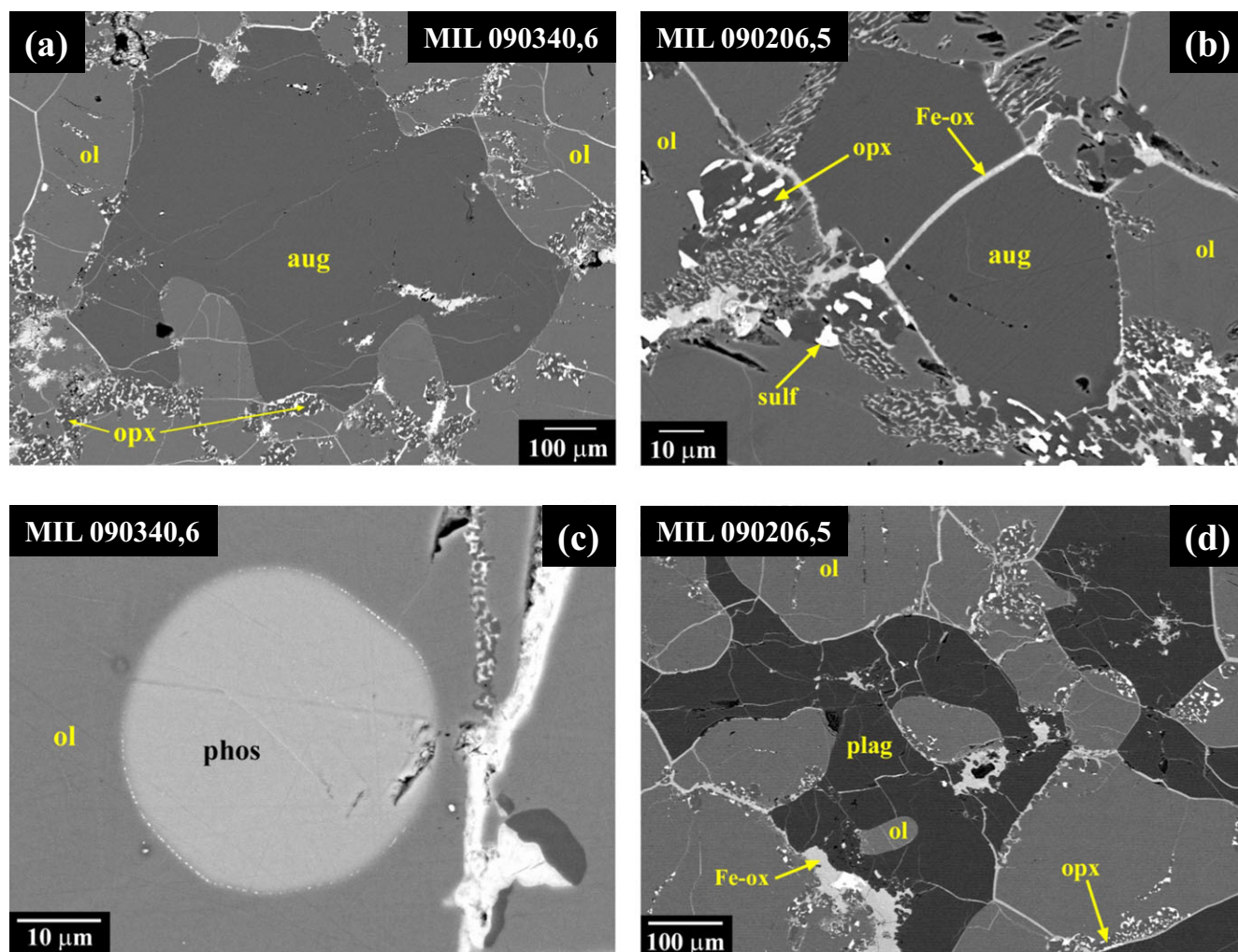


Fig. 2. BEI of MIL 090340 and MIL 090206. a) The only grain of augite in section MIL 090340,6. b) Grain of augite in nonpoikilitic area of MIL 090206,5. Olivine-augite contacts are lined with fine-grained intergrowths of orthopyroxene plus metal, sulfide (sulf), and Fe-oxides (presumably altered metal and/or sulfide). c) The only grain of phosphate (phos) observed in MIL 090340,6. d) Grains of plagioclase (plag), with intergranular and partly poikilitic morphologies, in MIL 090206,5. Other phase labels as in Fig. 1. (Color figure can be viewed at wileyonlinelibrary.com.)

None of the chromite analyses indicate a significant amount of Fe_2O_3 (calculation using the method of Droop 1987). The phosphate grain (Fig. 2c) is chlorapatite, with ~ 5.5 wt% Cl, 0.25 wt% F, and 1 wt% FeO (Table 4).

All sulfides analyzed are FeS (Table 5). Both the “large” grains of metal along grain boundaries and the small metal grains in grain boundary intergrowths with orthopyroxene (Fig. 3e) have 6–7 wt% Ni and 0.6 wt% Co (Table 5). In contrast, the euhedral metal grain enclosed in chromite (Fig. 3a) has ~ 18.7 wt% Ni and 1.3 wt% Co (Table 5).

MIL 090206

Compositions of olivine grains in nonpoikilitic areas of MIL 090206 range from Fo 70 to 74.5, with an average value of $\text{Fo } 72.3 \pm 0.1$ (Table 1, Fig. 5a). They

contain 0.08 ± 0.1 wt% CaO and 0.04 ± 0.01 wt% Cr_2O_3 , with molar $\text{Fe}/\text{Mn} = 50.8 \pm 2.3$ (Table 1, Fig. 6). Compositions of olivine chadocysts in the orthopyroxene oikocyst range from Fo ~ 75 to 77, with an average value of $\text{Fo } 76.1 \pm 0.6$ (Table 1, Fig. 5a). They contain 0.06 ± 0.2 wt% CaO, with Cr_2O_3 contents below detection limit and molar $\text{Fe}/\text{Mn} = 48.5 \pm 2.0$ (Table 1, Fig. 6). Eight olivine grains (both chadocysts in orthopyroxene and grains in the nonpoikilitic area) were examined for zonation (e.g., Fig. 5b). All showed slight reverse zonation from centers toward grain boundaries, or toward internal patches of the orthopyroxene+opaques assemblage, with Fo increasing by up to ~ 2 units (Fig. 5b).

The composition of the augite is Wo 43.3 ± 0.2 , mg# 81.3 ± 0.2 , with ~ 0.3 wt% TiO_2 , 0.6 wt% Al_2O_3 ,

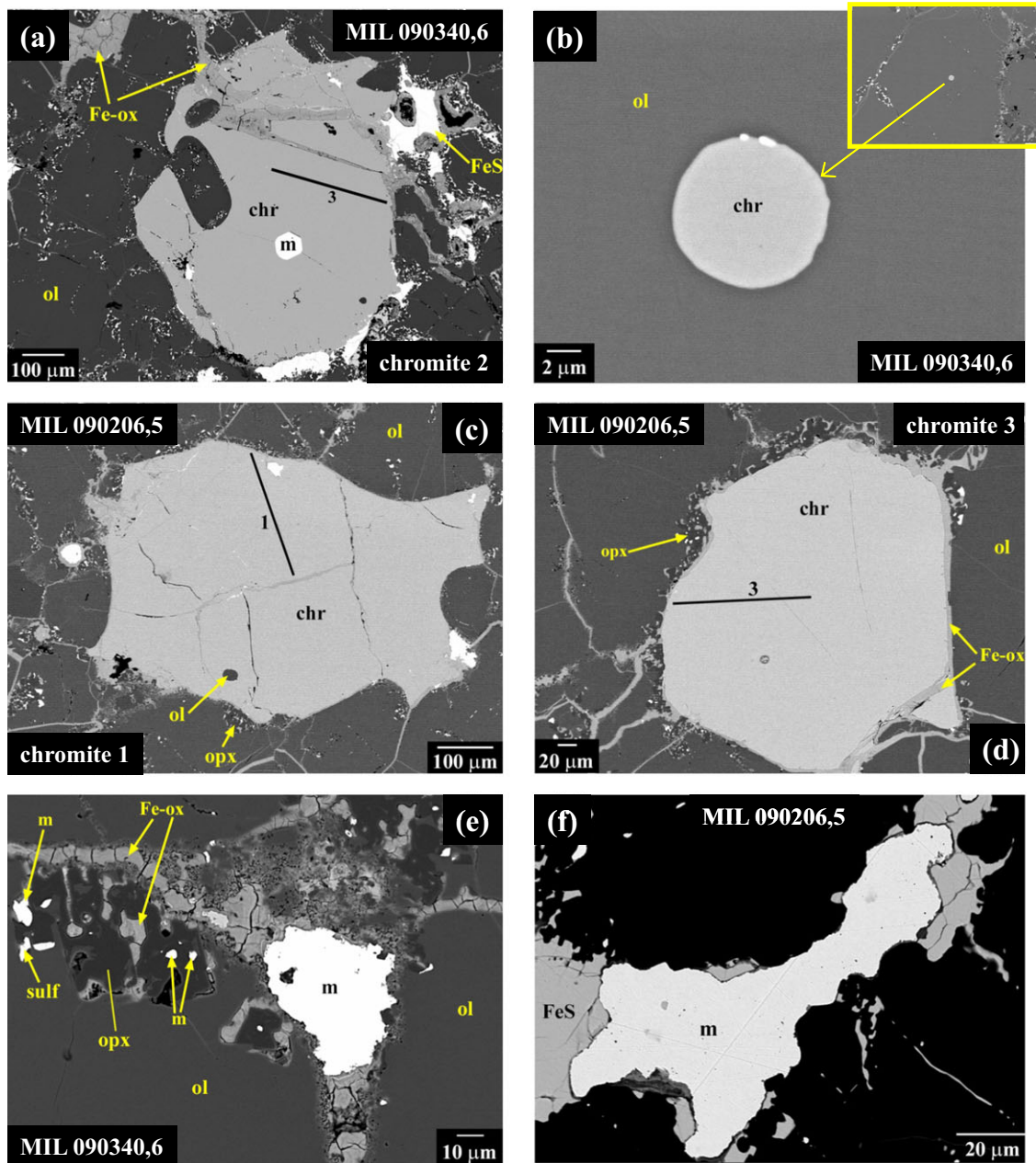


Fig. 3. BEI of MIL 090340 and MIL 090206. (a, c, and d) show large, intergranular chromite (chr) grains. Note subhedral inclusion of metal (m) in chromite in (a). Locations of compositional profiles given in Fig. 8 are marked by lines and numbers. b) Small, round chromite grain enclosed in olivine in MIL 090340. e) Patch of metal and Fe-oxides along grain boundary in MIL 090340. f) Patch of metal and sulfide (FeS) along grain boundary in MIL 090206. Other phase labels as in Figs. 1 and 2. (Color figure can be viewed at wileyonlinelibrary.com.)

0.75 wt% Cr_2O_3 and 0.5 wt% Na_2O (Table 2, Fig. 7). The composition of the orthopyroxene oikocryst is $\text{Wo } 2.2 \pm 0.01$, $\text{mg}\# 74.4 \pm 0.01$, with ~ 0.1 wt% TiO_2 , 0.2 wt% Al_2O_3 , and 0.3 wt% Cr_2O_3 (Table 2, Fig. 7a). The composition of orthopyroxene in grain boundary intergrowths is $\text{Wo } \sim 1.1$, $\text{mg}\# \sim 79$, with ~ 0.1 wt% Cr_2O_3 , and TiO_2 , Al_2O_3 and Na_2O contents near or below detection limit (Table 2).

Large chromite grains in nonpoikilitic areas have nearly uniform compositions of $\text{fe}\# \sim 73\text{--}75$ and $\text{Cr}\# 84.2\text{--}84.3$, with ~ 2.4 wt% TiO_2 and 0.7 wt% V_2O_3 (Table 3; Figs. 8 and 9). They show slight normal zonation, with outermost rims having $\text{fe}\#$ up to 3 units higher than grain interiors (Fig. 8). The small round chromite grains are unzoned. They have $\text{Cr}\#$ and TiO_2 and V_2O_3 contents similar to those of the large chromites,

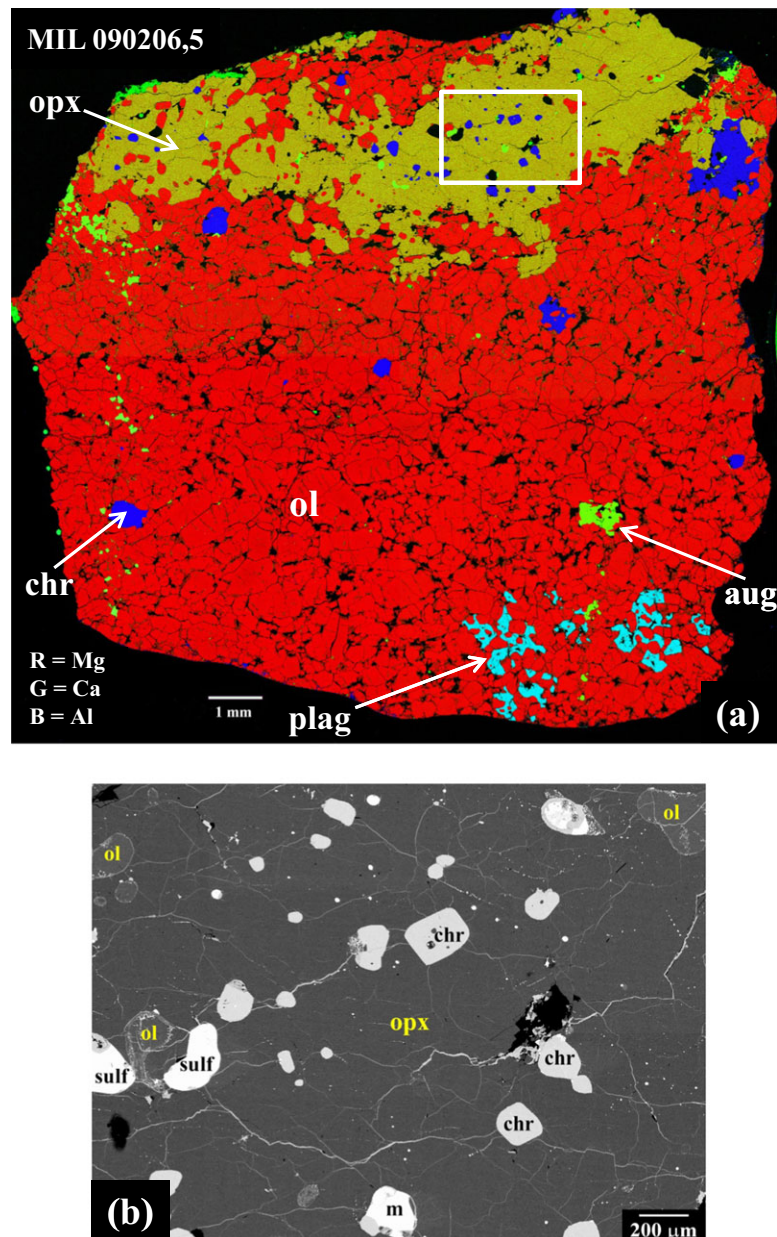


Fig. 4. a) Combined three-element X-ray map of section MIL 090206,5. Red = Mg, green = Ca, blue = Al. Olivine = red; augite = bright green; chromite = bright blue; plagioclase (plag) = cyan; orthopyroxene = yellowish green. Top part of section is dominated by single oikocryst of orthopyroxene containing rounded chadocrysts of olivine, chromite, augite, sulfide (sulf), and metal. Plagioclase is concentrated only in lower right of section. b) BEI of part of poikilitic area, outlined by white box in (a). Other phase labels as in Figs. 1 and 2.

but are more ferroan with $fe\# \sim 80.5$ (Table 3). Chromite chadocrysts in the orthopyroxene oikocryst have $Cr\#$ and TiO_2 and V_2O_3 contents similar to those of the large chromites, but are slightly more magnesian with $fe\# \sim 72-74$ (Table 3). One large chromite grain that is partially enclosed by orthopyroxene at the edge of the oikocryst (upper right, Fig. 4a) is similar to the chadocrysts in composition and appears to be unzoned (Table 3, grain

5; Fig. 8). None of the chromite analyses indicate a significant amount of Fe_2O_3 (calculation using the method of Droop 1987).

Plagioclase is homogeneous $An\ 17.5 \pm 0.3$, $Or\ 3.3 \pm 0.3$ (Table 4). All analyzed sulfides are FeS (Table 5). The “large” grains of metal along grain boundaries (e.g., Figs. 3e and 3f) have ~ 6 wt% Ni and 0.6 wt% Co (Table 5).

Table 1. Compositions of olivine in MIL 090340,6 and MIL 090206,5.

	MIL 090340,6		MIL 090340,6		MIL 090206,5		MIL 090206,5	
	Grain cores		Olivine grain 5		Grain cores in nonpoikilitic areas		Chadocrysts in opx oikocryst	
	Avg. (61)	Stdev	Interior	Edge	Avg. (95)	Stdev	Avg. (33)	Stdev
SiO ₂	37.1	0.3	37.3	36.6	37.8	0.4	38.4	0.6
Cr ₂ O ₃	0.04	0.01	0.02	0.04	0.04	0.01	bdl	
FeO	26.2	0.5	26.3	27.6	25.2	0.8	22.1	0.5
MgO	36.6	0.5	36.8	35.8	36.8	0.7	39.5	0.5
MnO	0.48	0.02	0.43	0.48	0.49	0.02	0.45	0.02
CaO	0.08	0.01	0.06	0.08	0.08	0.01	0.06	0.02
Total	100.5		100.9	100.6	100.6		100.6	
Fe/Mg ^a	0.402	0.012	0.397	0.428	0.384	0.020	0.315	0.010
Fo ^b	71.3	0.6	71.6	70.0	72.3	1.0	76.1	0.6
Fe/Mn ^a	54.0	1.7	56.6	53.9	50.8	2.3	48.5	2.0

^aMolar values.^bmolar Mg/(Fe+Mg).

Grain Boundary Intergrowths in MIL 090340 and MIL 090206

The grain boundary intergrowths of orthopyroxene + opaques have similar properties in MIL 090340 and MIL 090206. They form linings along olivine grain boundaries, occurring on one or both sides of the boundary (commonly separated by a narrow strip of Fe-oxide that marks the actual grain boundary) and ranging from ~5 to 50 μm in width (Figs. 1b, 1d, 2a, 2b, and 2d). They also occur as veins (as narrow as a few μm) extending into olivine grains from the grain boundaries, as apparently isolated patches within the grains, and as rims or patches around inclusions in the grains. In MIL 090206, they also occur as rims around chadocrysts of olivine in the orthopyroxene oikocryst (e.g., Fig. 4b). The opaque mineral grains within the orthopyroxene typically show strong preferred alignment, indicating crystallographic control by their hosts (Figs. 10 and 11). In many cases, the intergrowth has a myrmekitic appearance, with the opaques showing wormlike or vermicular morphology (Figs. 10 and 11).

The opaques are dominantly Fe-oxides/hydroxides (Fig. 10), which appear to be pseudomorphs (terrestrial weathering products) after metal or sulfide. Preserved sulfides are common, particularly among the larger opaque grains (Figs. 10a–c and 11a–c), and in some areas they are more abundant than Fe-oxides (Figs. 11a–c). In particular, in very narrow veins of these intergrowths crosscutting olivine grains, Fe-oxides are sometimes absent and in those cases the only opaques are Fe-sulfide (e.g., Fig. 10d). Metal is rare. Nevertheless, we observed a few areas in which the larger opaque grains in these intergrowths are dominantly Fe,Ni metal (e.g., Figs. 11d–f).

Cr Valences

Table 6 summarizes the Cr valence results for eight olivine grains in MIL 090340 and nineteen grains in MIL 090206, as well as five grains in each of the three brachinites. The valence means (\pm standard deviations) for the three brachinites, Brachina, Nova 003, and Hughes 026, were 2.50 ± 0.07 , 2.70 ± 0.06 , and 2.69 ± 0.04 , respectively. Brachina's valence is significantly more reduced than those of the other two brachinites, reinforcing the view that Brachina is an outlier relative to the "type" properties of this meteorite group (Goodrich et al. 2011; Greenwood et al. 2012; Gardner-Vandy et al. 2013).

Olivine from the two texturally distinct areas in MIL 090206, chadocrysts in the large orthopyroxene oikocryst and grains in nonpoikilitic areas, had significantly different Cr valence. Means for these two locations were 2.74 ± 0.03 and 2.59 ± 0.07 , respectively. MIL 090340 olivine grains had a mean valence of 2.57 ± 0.06 , essentially identical to the nonpoikilitic areas in MIL 090206.

We have previously reported Cr valence states of olivine in 11 ureilites covering the entire observed range of ureilite Fo values (Goodrich et al. 2013a). Here, we analyzed an additional five low-Fo, chromite-bearing ureilites, to provide a larger database for comparison with MIL 090340, MIL 090206, and brachinite samples. The valence means (\pm standard deviations) for the five additional ureilites reported here are summarized in Table 7. Shisr 007, META 78008, LAP 02382, HaH 064, and PCA 82506 yielded Cr valences of 2.22 ± 0.04 , 2.28 ± 0.03 , 2.25 ± 0.04 , 2.25 ± 0.06 , and 2.15 ± 0.02 , respectively.

The valences for MIL 090340 and MIL 090206 are compared in Fig. 12 with the valences for the three

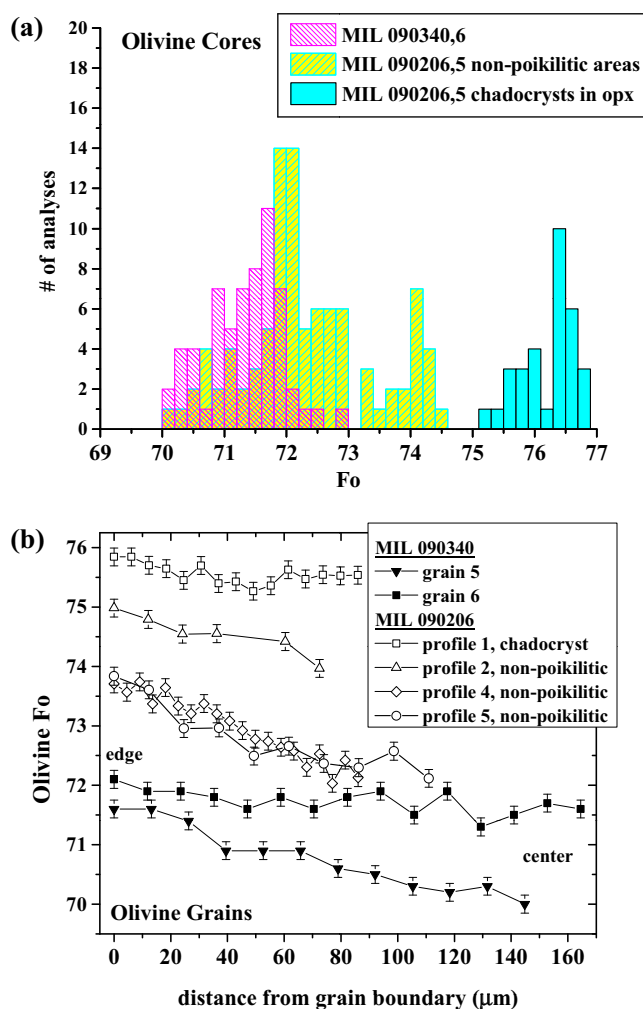


Fig. 5. a) Histogram of olivine compositions (Fo = molar Mg/[Mg+Fe]) in MIL 090340 and MIL 090206. b) Profiles of Fo in olivine grains in MIL 090340 and MIL 090206. Each profile begins at the edge of a grain and ends near its center. In MIL 090340, most grains show no significant zonation, but a few show slight reverse zonation. In MIL 090206, most grains examined show slight reverse zonation. Error bars indicate analytical error on Fo. (Color figure can be viewed at wileyonlinelibrary.com.)

brachinites and sixteen ureilites. The three brachinites and two MIL samples extend the previously observed ureilite valence systematic (lower Fo corresponding to more oxidized Cr) to lower Fo, suggesting that the Cr valences in the brachinites and MIL samples are redox-controlled, as was concluded for the ureilites (Goodrich et al. 2013a). Similar redox-controlled trends produced by the transition between Cr^{2+} and Cr^{3+} are observed in laboratory experiments (e.g., Berry and O'Neill 2004) where redox equilibrium between the two species is found to lie slightly more oxidized than IW. The olivine grains in the brachinites have more oxidized Cr and higher Fe concentrations than those in any of the

analyzed ureilites. That is, brachinites and ureilites are distinguishable on the “Cr valence versus Fo” plot (Fig. 12). MIL 090340 and MIL 090206 lie close to the brachinite region on this plot.

The more oxidized valence and higher Fo for olivine from the pyroxene oikocryst in MIL 090206 (compared with the nonpoikilitic regions of this sample) are intriguing. The relationship between the two components does not follow the apparent redox-controlled systematic of the overall sample suite, which indicates that higher Fo should be associated with more reduced Cr. Since the olivine grains in the oikocryst are relatively small ($\sim 200 \mu\text{m}$), we tested the possibility that stray signal from the host pyroxene might be interfering with the olivine measurement. The maximum orthopyroxene contribution is $< 10\%$ based on the relative Ti $K\alpha$ signals, and the orthopyroxene valence (2.51 ± 0.05 ; measured at the labeled positions “opx” and “opx1” in Fig. S2) based on the olivine calibration was determined to be slightly more reduced than that of the olivine. Thus, we estimate that the maximum effect of orthopyroxene overprinting would be a 0.04 reduction in the olivine Cr valence. This effect cannot account for the valence contrast between the two olivine populations.

Oxygen Isotope Ratios

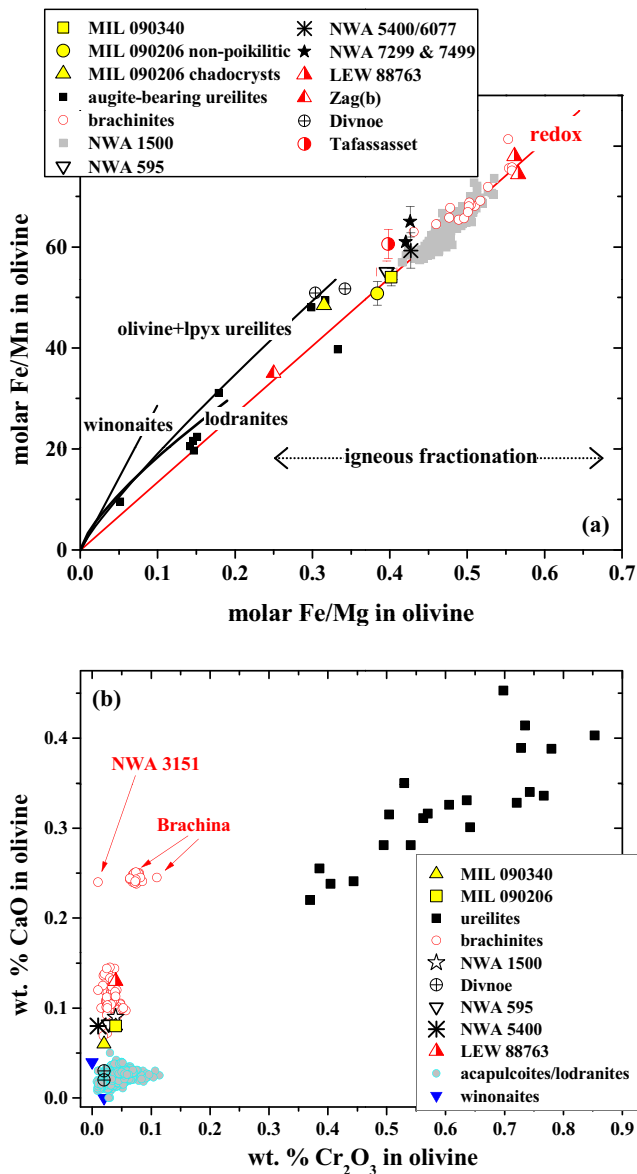
A total of 16 spot analyses of oxygen isotope compositions were obtained from eight different olivine grains in thin section MIL 090340,6. The data do not show significant variability in $\delta^{18}\text{O}$, $\delta^{17}\text{O}$, and $\Delta^{17}\text{O}$ beyond the reproducibility of standard olivine analyses (Table S4 in supporting information). The average values for the 16 analyses were $\delta^{18}\text{O} = 5.08 \pm 0.30\text{‰}$, $\delta^{17}\text{O} = 2.44 \pm 0.21\text{‰}$, and $\Delta^{17}\text{O} = -0.20 \pm 0.12\text{‰}$ (Fig. 13), and can be taken as very close to those of the bulk rock, considering that the modal abundance of olivine in MIL 090340 is 97%.

DISCUSSION

Comparison of MIL 090340 and MIL 090206 with Ureilites, Brachinites, and Other Olivine-Rich Primitive Achondrites

Modal Abundances

MIL 090340 was originally investigated by Warren and Rubin (2012) and Goodrich et al. (2012) as a potentially important new ureilite. If it was a ureilite, as originally classified (Antarctic Meteorite Newsletter 2011), it would be an exceptionally ferroan one, extending the known range of ureilite Fo contents. The presence of chromite in both MIL 090340 and MIL



090206, and of phosphate in MIL 090340, distinguishes these samples from most ureilites. However, as discussed by Goodrich et al. (2006) with reference to NWA 1500 (a brachinite-like achondrite originally thought to be a ureilite), these features would be expected in an exceptionally ferroan (more oxidized) ureilite. Such a ferroan ureilite might also be expected to contain augite rather than low-Ca pyroxene (Goodrich et al. 2004, 2006).

Modal abundances of major silicates (other than olivine) in MIL 090340 and MIL 090206 are compared in Fig. 14 with those of brachinites and brachinite-like achondrites, augite-bearing ureilites, winonaites, acapulcoites and lodranites, and several ungrouped achondrites. MIL 090340 plots in the field of augite-

Fig. 6. a) Plot of molar Fe/Mg versus Fe/Mn in olivine in MIL 090340 and MIL 090206, compared with ureilites (olivine + low-Ca pyroxene [lpvx] ureilites shown by black line; augite-bearing ureilites by solid black squares), lodranites, winonaites, brachinites and brachinite-like achondrites, and some ungrouped achondrites. Each group shows a characteristic trend of near-constant Mn/Mg ratio, which is a redox (reduction-oxidation) trend rather than an igneous fractionation trend. Brachinites and most brachinite-like achondrites have more ferroan olivine (higher Fe/Mg ratio, lower Fo) than any ureilites, lodranites, or winonaites. MIL 090340 and the nonpoikilitic regions of MIL 090206 plot along the brachinite clan trend, with compositions similar to brachinite-like achondrite NWA 595. The olivine chadocrysts in MIL 090206 are more magnesian (lower Fe/Mg), but have Fe/Mn ratio similar to that of olivine in the nonpoikilitic regions. b) Plot of wt% CaO versus Cr₂O₃ in olivine in MIL 090340 and MIL 090206, compared with ureilites, brachinites, and various brachinite-like achondrites, winonaites, and acapulcoites/lodranites. Brachinite data from Nehru et al. (1983), Warren and Kallemeyn (1989), Goodrich and Righter (2000), Mittlefehldt et al. (2003), and Goodrich et al. (2011). Data for NWA 1500 from Goodrich et al. (2006); NWA 595 from Goodrich et al. (2011); NWA 5400/6077 from Gardner-Vandy et al. (2013); NWA 7299 and NWA 7499 from Meteoritical Bulletin Database; Zag(b) from Delaney et al. (2000); Divnoe from Petaev et al. (1994); Tafassasset from Gardner-Vandy et al. (2012); LEW 88763 from Gardner-Vandy (2012) and Day et al. (2015). For sources of ureilite, lodranite, and winonaite data, see fig. 5 of Goodrich et al. (2011). (Color figure can be viewed at wileyonlinelibrary.com.)

bearing ureilites and the field of brachinites. It is distinguished from the former, however, by its very low augite/olivine ratio. MIL 090206,6 contains much more orthopyroxene than augite, and plots in the field of lodranites, as well as the broad field of brachinite-like achondrites.

The low abundances of sulfide and metal in both MIL 090340 and MIL 090206 are consistent with abundances of these phases in either brachinites or ureilites, and are lower than typical abundances of these phases in acapulcoites, lodranites, or winonaites (see fig. 2 of Goodrich et al. 2011).

The grain boundary orthopyroxene+opaque assemblages in MIL 090340 and MIL 090206 have some similarities to the characteristic reduction rims on olivine in ureilites. However, they are more similar to grain boundary orthopyroxene+opaque assemblages found in many brachinites and brachinite-like achondrites. A detailed comparison of these intergrowths with ureilite reduction rims, and a discussion of their possible origin, are given in a later section.

Textures and Grain Sizes

The textures and grain sizes of the olivine-rich areas of MIL 090340 and MIL 090206 are consistent with those of either ureilites or brachinites, and also with

Table 2. Compositions of pyroxenes in MIL 090340 and MIL 090206

	MIL 090340,6			MIL 090206,5					
	Primary augite		Grain boundary opx (1)	Primary augite		Opx oikocryst		Grain boundary opx	
	Avg. (2)	Stdev		Avg. (34)	Stdev	Avg. (44)	Stdev	Avg. (6)	Stdev
SiO ₂	53.2	0.21	54.1	54.0	0.4	54.8	0.4	53.0	0.9
TiO ₂	na		0.04	0.26	0.02	0.12	0.01	0.04	
Al ₂ O ₃	0.71	0.04	0.04	0.61	0.03	0.24	0.02	0.09	0.05
Cr ₂ O ₃	0.75	0.03	0.11	0.75	0.04	0.29	0.13	0.11	0.03
FeO	6.6	0.4	15.6	6.7	0.10	16.6	0.3	15.0	0.4
MgO	16.4	0.1	30.4	16.3	0.1	27.0	0.2	31.5	0.6
MnO	0.23	0.04	0.42	0.21	0.01	0.40	0.02	0.42	0.02
CaO	20.8	0.4	0.52	21.3	0.1	1.11	0.02	0.64	0.12
Na ₂ O	0.45	0.07	bdl	0.47	0.02	bdl		bdl	
Total	98.3		101.3	100.7		100.6		100.8	
Wo ^a	42.6	1.0	0.94	43.3	0.2	2.2	0.01	1.1	0.2
mg ^{#b}	81.6	0.8	77.6	81.3	0.2	74.4	0.01	79.0	0.5

na = not analyzed.

^amolar Ca/(Ca+Mg+Fe).

^bmolar Mg/(Mg+Fe).

those of some lodranites. The poikilitic texture of the orthopyroxene-rich area of MIL 090206 is not unlike that of some augite-bearing ureilites, but also resembles poikilitic pyroxene-rich areas in brachinite-like achondrites NWA 595 (Goodrich et al. 2011) and NWA 7605 (Irving et al. 2013). The intergranular morphologies of augite and plagioclase grains in MIL 090340 and MIL 090206 are not seen in ureilites, but are similar to textures shown by these minerals in brachinites and brachinite-like achondrites, as well as some acapulcoites.

Mineral Compositions

The Fo values of olivine in MIL 090340 and MIL 090206 are lower than those of olivine in any main group ureilite. They are slightly higher than those of the most magnesian brachinites, but similar to brachinite-like achondrites (especially NWA 595 and NWA 1500), as well as the ungrouped achondrite Tafassasset. The Fe/Mg-Fe/Mn compositions of olivine in MIL 090340 and in the nonpoikilitic areas of MIL 090206 (Fig. 6a) plot along the trend defined by brachinites and several brachinite-like achondrites, clearly distinguished from the Fe/Mg-Fe/Mn trend of olivine + low-Ca pyroxene ureilites by higher Fe/Mg ratios and higher Mn/Mg ratio. The augite-bearing ureilites have higher Fe/Mg ratios than olivine + low-Ca pyroxene ureilites of similar Fe/Mn ratio, but still have lower Fe/Mg ratio than the MIL samples. Olivine chadocrysts in the poikilitic region of MIL 090206 have Fe/Mn ratio similar to that of olivine in the nonpoikilitic region, but lower Fe/Mg (i.e., higher Fo), and plot significantly off the brachinite trend.

In terms of Cr₂O₃ and CaO contents, olivines in MIL 090340 and MIL 090206 are within the field of brachinites, at the low end of the range for CaO, and very similar to brachinite-like meteorites NWA 1500, NWA 595, and NWA 5400 (Fig. 6b). They are well distinguished from olivines in ureilites, which have much higher Cr₂O₃ contents than any other olivine-rich primitive achondrites and higher CaO contents than all but a few brachinites. They are also distinguished from olivines in acapulcoites, lodranites, and winonaites, which have lower CaO contents (Fig. 6b).

Major element compositions of augite and primary orthopyroxene in MIL 090340 and MIL 090206 are within the fields of those in brachinites and similar to those in brachinite-like meteorites NWA 1500, NWA 595, and NWA 5400 (Fig. 7). They are clearly distinguished from pyroxenes in ureilites, which have higher Wo in orthopyroxene and lower Wo in augite, as well as being more magnesian (Fig. 7). They are also distinguished from pyroxenes in acapulcoites, lodranites, and winonaites, which are more magnesian (Fig. 7). Augite in MIL 090340 and MIL 090206 has Cr₂O₃ and Al₂O₃ contents within the range of those in brachinites and brachinite-like achondrites NWA 595, NWA 5400, and NWA 1500, and well distinguished from the much higher values in augite-bearing ureilites (Fig. 7b).

Chromites in MIL 090340 and MIL 090206 have *fe*#s higher than those of chromites in ureilites, winonaites, and most acapulcoites and lodranites, and similar to those of chromites in brachinites and brachinite-like achondrites (Fig. 9a). Their *Cr*#s are consistent with those of chromites in some brachinites and brachinite-like achondrites; i.e., higher than those in

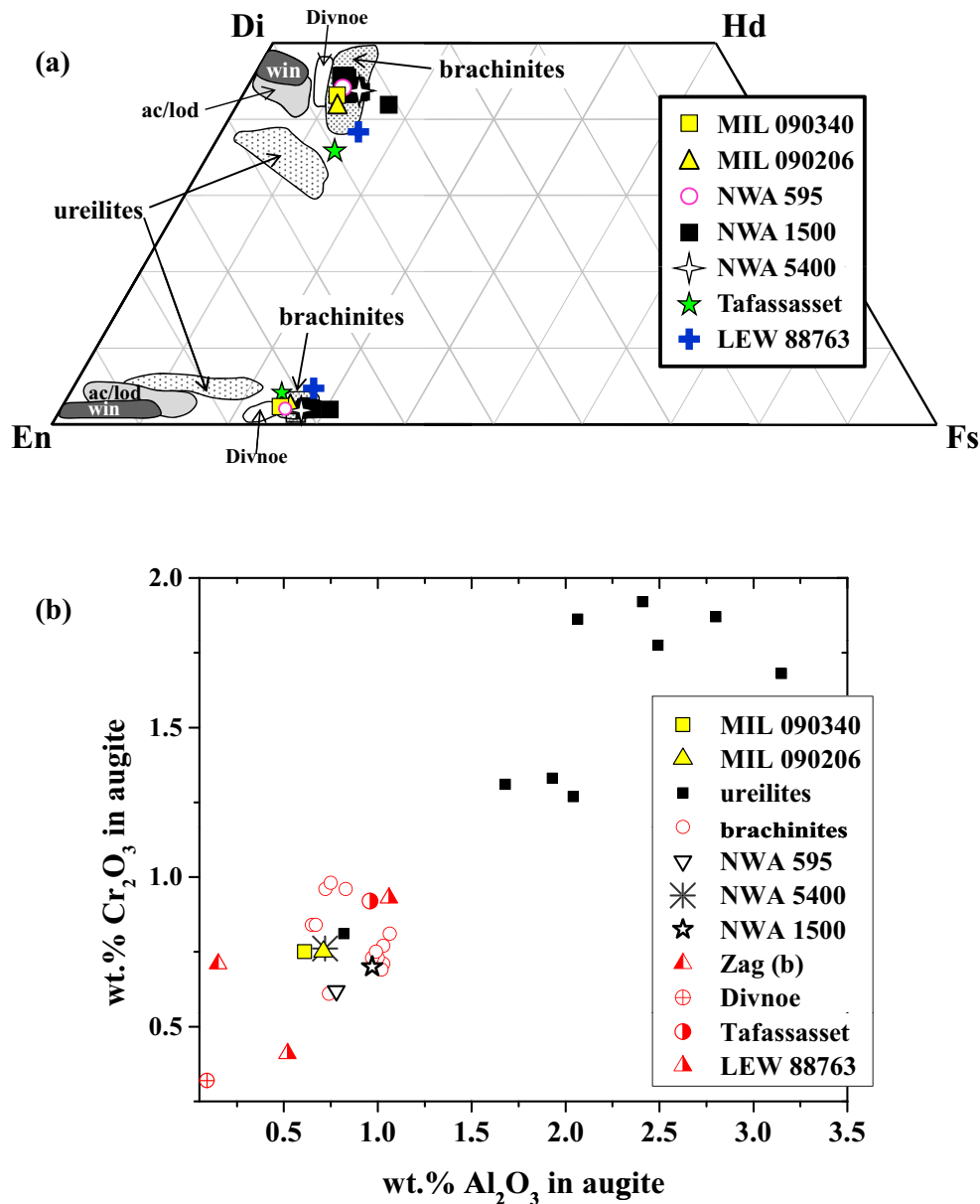


Fig. 7. a) Pyroxene quadrilateral showing compositions of pyroxenes (augite and primary orthopyroxene) in MIL 090340 and MIL 090206 compared with those in ureilites, brachinites, various brachinite-like achondrites, winonaites (win), acapulcoites/lodranites (ac/lod), and some ungrouped achondrites. b) Plot of wt% Al₂O₃ versus Cr₂O₃ in augite in MIL 090340 and MIL 090206, compared with augite-bearing ureilites, brachinites, and various brachinite-like achondrites. References are as given in fig. 7 of Goodrich et al. (2011), with the addition of: Tafassasset from Gardner-Vandy (2012); LEW 88763 from Gardner-Vandy (2012) and Day et al. (2015); Zag(b) from Delaney et al. (2000); NWA 5400 from Gardner-Vandy et al. (2013). Orthopyroxene in MIL 090340 from Warren and Rubin (2012). (Color figure can be viewed at wileyonlinelibrary.com.)

ureilites and most winonaites, and similar to those in acapulcoites and lodranites (Fig. 9a). Their TiO₂ contents (Fig. 9b) are significantly higher than those of chromites in ureilites, acapulcoites and lodranites, and winonaites, and are similar to those of some brachinites and brachinite-like achondrites (though higher than those of others). The V₂O₃ contents (Fig. 9b) are similar

to those of most brachinites and brachinite-like achondrites, and higher than those of chromites in ureilites, winonaites, and many acapulcoites and lodranites.

Plagioclase in MIL 090206 (An ~18) is slightly more sodic than plagioclase in brachinites and brachinite-like achondrites (An 22–40) and falls within the ranges for

Table 3. Compositions of selected chromite in MIL 090340,6 and MIL 090206,5

MIL 090340,6												
Size	Chromite grain 1			Chromite grain 2			Chromite grain 3			Grain 4	Grain 5	Grain 6
	250 μm			550 μm			400 μm			10 μm	25 μm	30 μm
	Interior			Interior			Interior			Small round	Small round	Small round
	Avg. (9)	Stdev	Rim	Avg. (36)	Stdev	Rim	Avg. (18)	Stdev	Rim			
SiO ₂	0.04	0.01	0.05	0.03	0.01	0.04	0.04	0.02	0.03	0.07	0.04	0.04
TiO ₂	2.44	0.03	2.30	2.41	0.03	2.38	2.42	0.05	2.42	2.22	2.31	2.25
Al ₂ O ₃	7.2	0.1	7.3	7.2	0.1	7.3	7.1	0.1	7.4	6.9	6.8	7.2
Cr ₂ O ₃	57.7	0.2	57.2	57.6	0.3	56.6	58.5	0.3	56.5	54.5	55.8	56.8
V ₂ O ₃	0.74	0.01	0.72	0.74	0.02	0.74	0.73	0.02	0.77	0.72	0.69	0.65
FeO	27.6	0.2	28.0	27.3	0.2	27.9	27.1	0.2	27.7	30.7	30.1	29.0
MgO	4.54	0.06	4.41	4.71	0.07	4.57	4.79	0.11	4.43	2.98	3.28	3.45
MnO	0.50	0.03	0.51	0.47	0.03	0.48	0.49	0.03	0.48	0.55	0.54	0.52
Total	100.7		100.5	100.5		100.0	101.3	0.3	99.8	98.7	99.6	100.0
fe#	77.4	0.3	78.1	76.5	0.3	77.4	76.1	0.5	77.9	85.3	83.7	82.5
mg#	22.6	0.3	21.9	23.5	0.3	22.6	23.9	0.5	22.1	14.7	16.3	17.5
Cr#	84.4	0.1	84.0	84.3	0.2	84.0	84.6	0.3	83.7	84.1	84.5	84.1
<i>Cations on basis of 32 oxygen</i>												
Si	0.010		0.014	0.009		0.011	0.011		0.009	0.020	0.012	0.010
Ti	0.506		0.478	0.501		0.497	0.499		0.506	0.477	0.492	0.474
Al	2.330		2.387	2.336		2.378	2.299		2.420	2.332	2.281	2.386
Cr	12.584		12.514	12.578		12.443	12.666		12.442	12.331	12.472	12.577
V	0.163		0.160	0.164		0.165	0.160		0.171	0.166	0.156	0.146
Fe	6.370		6.478	6.303		6.494	6.216		6.464	7.357	7.118	6.803
Mg	1.865		1.819	1.938		1.894	1.953		1.839	1.270	1.382	1.441
Ca	0.000		0.000	0.000		0.000	0.000		0.000	0.000	0.000	0.000
Mn	0.117		0.119	0.111		0.112	0.114		0.112	0.134	0.129	0.124
SUM	23.946		23.977	23.952		23.999	23.928		23.968	24.088	24.042	23.961
Ol-sp T ^a	901		888	914		898	921		890	775	802	819

acapulcoites, lodranites, and winonaites (see summary in Goodrich et al. 2011; Fig. 9; see Day et al. [2012] and Gardner-Vandy et al. [2013] for more recent data).

The composition of the Cl-apatite in MIL 090340 is similar to compositions of apatites in Brachina (Nehru et al. 1983) and NWA 1500 (Goodrich et al. 2006), and consistent with reports that the phosphate in other brachinites is Cl-apatite.

The sulfides in MIL 090340 and MIL 090206 are troilite, consistent with either brachinites or ureilites. However, brachinites contain only one sulfide phase, troilite, whereas ureilites commonly contain both troilite and various Cr-rich sulfides (Goodrich et al. 2013b). Thus, in terms of sulfide phases, MIL 090340 and MIL 090206 are more like brachinites than ureilites. Because metal is rare in brachinites, there are few reports of its compositions. The “large” metal grains in MIL 090340 and MIL 090206 have Ni contents (~6 wt%) within the range of metal in ureilites, but with a lower Ni/Co ratio (Goodrich et al. 2013b). The euhedral inclusion of metal in chromite in MIL 090340 has Ni and Co contents similar to those of metal in brachinite-like achondrite NWA 5400 (Day et al. 2012).

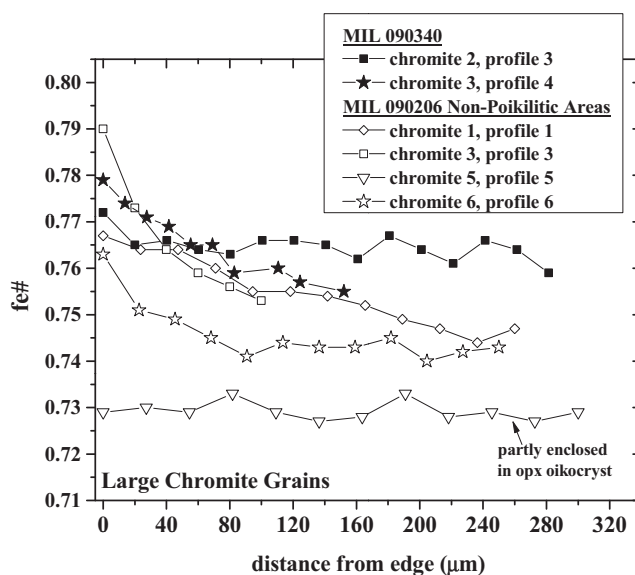


Fig. 8. Profiles of fe# (=molar Fe/[Mg+Fe]) in large chromites in MIL 090340 and the nonpoikilitic area of MIL 090206. All profiles begin at the edge of a grain and end near its center. The locations of some of these profiles are marked on the BEI in Fig. 3. Typical errors on fe# for these profiles (calculated from analytical errors on Fe and Mg) are ±~0.005.

Table 3. *Continued.* Compositions of selected chromite in MIL 090340,6 and MIL 090206,5

MIL 090206,5												
Size	Chromite 1 525 μm			Chromite 3 275 μm			Chromite 5 800 μm			Chromite 2 35 μm	Chromite 7a 105 μm	Chromite 7c 100 μm
	Interior			Interior			Interior			Small round	Chadocryst	Chadocryst
	Avg. (9)	Stdev	Rim	Avg. (6)	Stdev	Rim	Avg. (11)	Stdev	Rim	Avg. (4)	Avg. (4)	Avg. (6)
SiO ₂	0.03	0.01	0.04	0.04	0.02	0.06	0.08	0.02	0.08	0.04	0.05	0.04
TiO ₂	2.40	0.03	2.24	2.35	0.05	2.40	2.39	0.06	2.39	2.33	2.38	2.41
Al ₂ O ₃	7.25	0.04	7.19	7.19	0.10	7.11	7.15	0.17	7.17	7.04	7.15	7.36
Cr ₂ O ₃	57.8	0.3	56.6	57.7	0.1	56.6	58.2	0.5	57.9	56.80	57.80	58.20
V ₂ O ₃	0.71	0.02	0.72	0.71	0.05	0.83	0.69	0.04	0.70	0.71	0.72	0.74
FeO	27.0	0.3	27.6	27.1	0.2	28.1	26.2	0.2	26.3	28.97	26.61	26.21
MgO	5.01	0.09	4.71	4.91	0.10	4.46	5.46	0.08	5.49	3.94	5.32	5.58
MnO	0.51	0.01	0.50	0.52	0.01	0.52	0.52	0.02	0.52	0.53	0.55	0.52
Total	99.0	0.2	98.0	98.9	0.2	98.4	99.1	0.5	98.9	98.7	99.0	99.4
fe#	75.1	0.5	76.7	75.6	0.3	77.9	72.9	0.2	72.9	80.5	73.7	72.5
mg#	24.9	0.5	23.3	24.4	0.3	22.1	27.1	0.2	27.1	19.5	26.3	27.5
Cr#	84.2	0.1	83.7	84.3	0.2	84.2	84.5	0.4	84.4	84.4	84.4	84.1
<i>Cations on basis of 32 oxygen</i>												
Si	0.007		0.012	0.010		0.016	0.021		0.021	0.010	0.014	0.012
Ti	0.495		0.469	0.488		0.503	0.492		0.493	0.489	0.492	0.495
Al	2.350		2.363	2.338		2.331	2.310		2.321	2.312	2.317	2.367
Cr	12.570		12.490	12.582		12.454	12.613		12.569	12.519	12.566	12.550
V	0.157		0.161	0.157		0.185	0.152		0.154	0.159	0.159	0.162
Fe	6.208		6.440	6.250		6.533	6.010		6.037	6.753	6.118	5.978
Mg	2.053		1.957	2.017		1.850	2.230		2.247	1.637	2.181	2.269
Ca	0.000		0.000	0.000		0.000	0.000		0.000	0.000	0.000	0.000
Mn	0.118		0.119	0.122		0.123	0.122		0.121	0.126	0.127	0.120
Zn	0.000		0.000	0.000		0.000	0.000		0.000	0.000	0.000	0.000
SUM	23.959		24.012	23.964		23.996	23.950		23.963	24.006	23.973	23.954
Ol-sp T ^b	920		894	913		879	953		953	841	888	902

^aOlivine-spinel equilibration temperature (in °C) assuming olivine = Fo 71.3, based on Wlotzka (2005).

^bOlivine-spinel equilibration temperature (in °C) assuming olivine = Fo 72.3 for nonpoikilitic areas and Fo 76.1 for chadocrysts, based on Wlotzka (2005).

Equilibration Temperatures

We calculated equilibration temperatures for MIL 090340 and MIL 090206 using the olivine-spinel thermometer of Wlotzka (2005) and the olivine-augite Ca-exchange thermometer of Köhler and Brey (1990), and also for MIL 090206 the two-pyroxene (augite + orthopyroxene) thermometer of Lindsley and Andersen (1983) as embedded in QUILF (Andersen et al. 1993). Results are shown in Fig. 15, compared with similarly calculated temperatures for ureilites, brachinites and brachinite-like achondrites, and some ungrouped achondrites. Olivine-chromite temperatures calculated using the large chromite grains in MIL 090340 and MIL 090206 range from 895 to 930 °C. These temperatures are similar to those of most brachinites (Brachina being the exception with higher temperatures of ~1000–1100 °C) and brachinite-like achondrites NWA 5400 and NWA 595

(Fig. 15a). Olivine-chromite temperatures calculated using the small, round chromite grains in olivine in MIL 090340 and MIL 090206 are lower (their small size may have allowed equilibration to lower temperatures), ~795–840 °C, and similar to those of Tafassasset, LEW 88763, and Divnoe. In contrast, primary chromites in ureilites yield significantly higher olivine-spinel temperatures of ~1040 to 1250 °C (Goodrich et al. 2014).

Olivine-augite Ca distribution temperatures (Köhler and Brey 1990) for brachinites and some brachinite-like achondrites, as well as those for augite-bearing ureilites, are all higher than their corresponding olivine-chromite temperatures, ~1000 °C for brachinites (again, Brachina gives higher temperatures of ~1150–1200 °C) and ~1200 °C for ureilites (Fig. 15b). The olivine-augite temperatures of MIL 090340 and MIL 090206 are ~930 °C, only slightly higher than their olivine-chromite

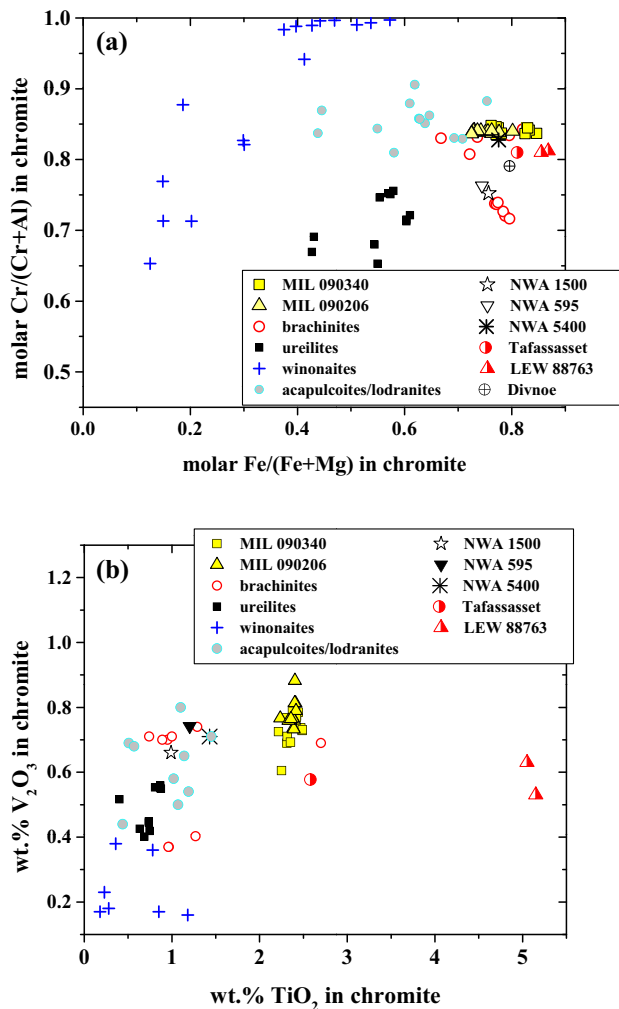


Fig. 9. a) Plot of Cr# (=molar Cr/[Cr+Al]) versus fe# (=molar Fe/[Mg+Fe]) for chromites in MIL 090340 and MIL 090206, compared with those in ureilites, brachinites and brachinite-like achondrites, winonaites, and acapulcoites/lodranites. Chromites in the MIL meteorites have higher Cr# and fe# than those in ureilites, and higher fe# than those in all other olivine-rich primitive achondrites except brachinites and brachinite-like achondrites. b) Plot of wt% V₂O₅ versus wt% TiO₂ in chromites in MIL 090340 and MIL 090206, compared with those in ureilites, brachinites and brachinite-like achondrites, winonaites, acapulcoites/lodranites, and some ungrouped achondrites. In terms of these elements, chromites in the MIL 090340 and MIL 090206 are similar only to those in some brachinites and brachinite-like achondrites. Sources of data: brachinites from Mittlefehldt et al. (2003), Gardner-Vandy et al. (2013), Warren and Kallemeyn (1989), Johnson et al. (1977) and Nehru et al. (1983); NWA 1500 from Goodrich et al. (2006); NWA 595 from this work; NWA 5400 from Gardner-Vandy et al. (2013); Divnoe from Petaev et al. (1994); Tafassasset from Gardner-Vandy et al. (2012); LEW 88763 from Gardner-Vandy (2012) and Day et al. (2015); ureilites from Goodrich et al. (2013a); winonaites and IAB silicates from Kimura et al. (1992) and Benedix et al. (2005); acapulcoites and lodranites from Mittlefehldt et al. (1996), Burrioni and Folco (2008), Folco et al. (2006), and Kimura et al. (1992). (Color figure can be viewed at wileyonlinelibrary.com.)

Table 4. Compositions of plagioclase and phosphate in MIL 090206 and MIL 090340.

	MIL 090206,5		MIL 090340,6	
	Plagioclase		Phosphate	
	Avg. (158)	Stdev	Avg. (4)	Stdev
SiO ₂	64.1	1.1	0.18	0.04
Al ₂ O ₃	22.7	0.3	0.00	0.00
FeO	0.33	0.95	1.05	0.18
MgO	0.03	0.02	0.00	0.00
MnO	0.03	0.02	0.09	0.03
CaO	3.66	0.08	52.40	0.35
Na ₂ O	9.17	0.09	0.45	0.03
K ₂ O	0.57	0.05	0.01	0.00
P ₂ O ₅	na		41.3	0.27
F			0.25	0.04
Cl			5.5	0.1
Total	100.6		101.3	
An	17.5	0.3		
Or	3.3	0.3		

temperatures, and closest to those of NWA 5400 and NWA 595 (Fig. 15b). The two-pyroxene temperature calculated for the poikilitic area (orthopyroxene oikocryst + augite chadocrysts) in MIL 090206 is ~930 °C, close to two-pyroxene temperatures for NWA 1500 (913 °C), NWA 595 (928 °C), and NWA 5400 (929 °C), whereas two-pyroxene temperatures for Tafassasset, Divnoe, and Zag (b) are ~1000–1100 °C, and those for augite-bearing ureilites are significantly higher at ~1200–1300 °C.

Thus, based on three different mineral thermometers, the equilibration temperatures of MIL 090340 and MIL 090206 are significantly lower than those of ureilites; similar to those of brachinites; and closest to those of brachinite-like achondrites NWA 1500, NWA 595, and NWA 5400.

Oxygen Isotopes

The oxygen isotope composition of olivine in MIL 090340, which must be very similar to that of the bulk rock because of the very high abundance of olivine, is not consistent with oxygen isotope compositions of ureilites (Fig. 13a), but is within the range of those of brachinites and brachinite-like achondrites (Fig. 13). Corder et al. (2014) reported an oxygen isotope composition for bulk MIL 090206 ($\delta^{18}\text{O} = -3.9$, $\Delta^{17}\text{O} = -0.15$) which is also within the range of those of brachinites and brachinite-like achondrites.

Cr Valences and Oxygen Fugacity Estimates

The valences of Cr in olivine in MIL 090340 and MIL 090206 are similar to those of the brachinites and significantly higher than those of ureilites, including the chromite-bearing ureilites (Fig. 12), which suggests that the parent bodies of MIL 090340, MIL 090206, and

Table 5. Compositions of sulfide and metal in MIL 090340 and MIL 090206.

	MIL 090340,6						MIL 090206,5					
	Sulfide		“Large” metal grains		Metal in grain boundary intergrowths		Euhedral metal grain in chromite		Sulfide		“Large” metal grains	
	Avg. (3)	Stdev	Avg. (9)	Stdev	Avg. (5)	Stdev	Avg. (2)	Stdev	Avg. (44)	Stdev	Avg. (32)	Stdev
Fe	63.1	0.2	93.1	0.3	91.6	0.2	80.1	0.2	63.5	0.3	94.0	0.4
Ni	bdl		6.3	0.2	6.6	0.3	18.7	0.04	bdl		6.0	0.3
Co	bdl		0.59	0.02	0.59	0.05	1.3	0.01	bdl		0.55	0.04
Cr	bdl		bdl		bdl		bdl		bdl		bdl	
S	36.6	0.0	bdl		bdl		bdl		36.7	0.1	bdl	
Total	99.7		100.1	0.3	98.9		100.4		100.3	0.3	100.6	

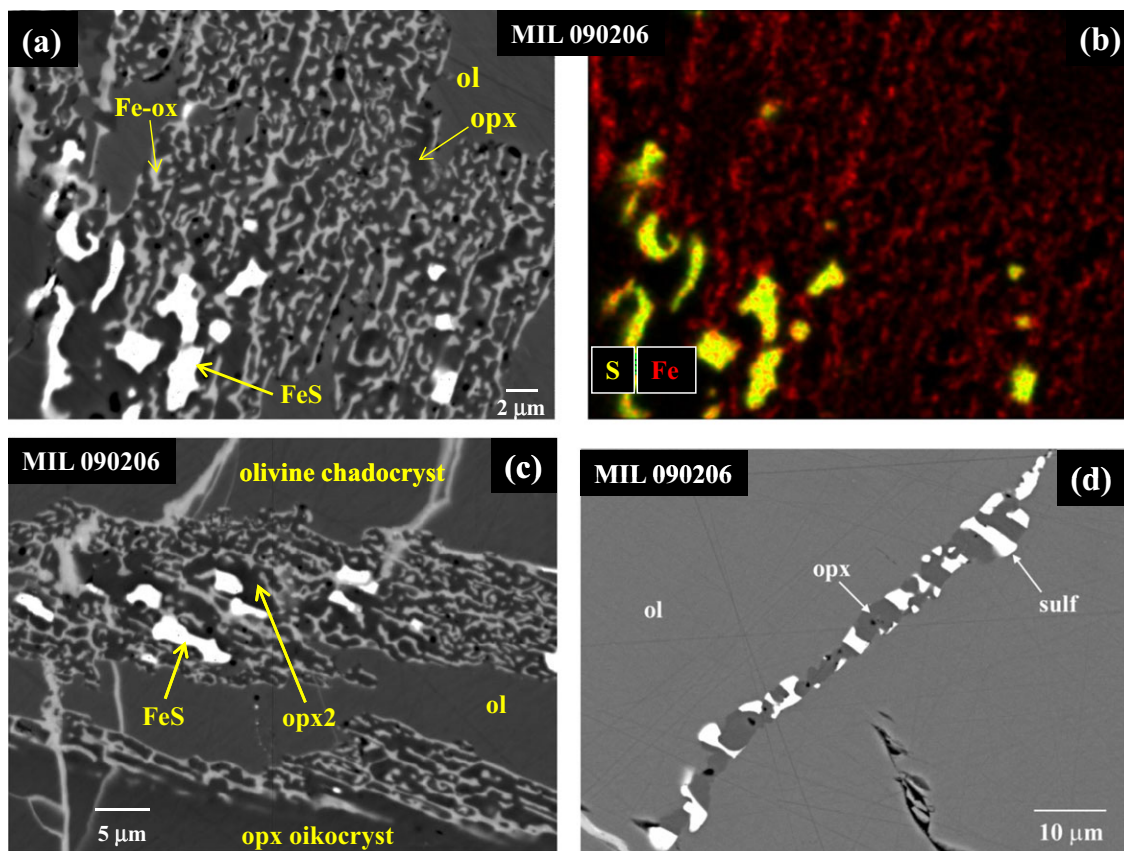


Fig. 10. Fine-grained intergrowths of orthopyroxene (opx) plus opaques along margins of, or as veins within, olivine grains in MIL 090206. a) BEI showing intergrowth in which the finer-grained opaques are dominantly Fe-oxides (Fe-ox), assumed to be terrestrial alteration of pre-existing metal or sulfide. A few larger grains (bright) are preserved sulfide (FeS). b) Combined Fe (red) and S (yellow) x-ray map of area in (a). c) Intergrowth along margin of olivine chadocryst in orthopyroxene. As in (a,b), opaques are dominantly Fe-oxide, with only a few larger grains of preserved sulfide. Orthopyroxene in intergrowth (opx2) is distinct in composition from the orthopyroxene oikocryst (see text). d) Vein in olivine, in which there is no alteration and all opaques are sulfide. In all images, note crystallographic control on shape and orientation of the opaque phase(s). Phase labels as in Figs. 1–4.

brachinites were more oxidized than the ureilite parent body. This inference can be quantified by estimating fO_2 values from the Cr valence measurements. Magmatic fO_2 values for ureilites were calculated by Goodrich

et al. (2013a) using the Hanson and Jones “Cr valence- fO_2 ” relationship (e.g., Equation 1 given above at 1200 °C). Values obtained for the chromite-lacking ureilites were very reducing, ranging from IW-1.9 to

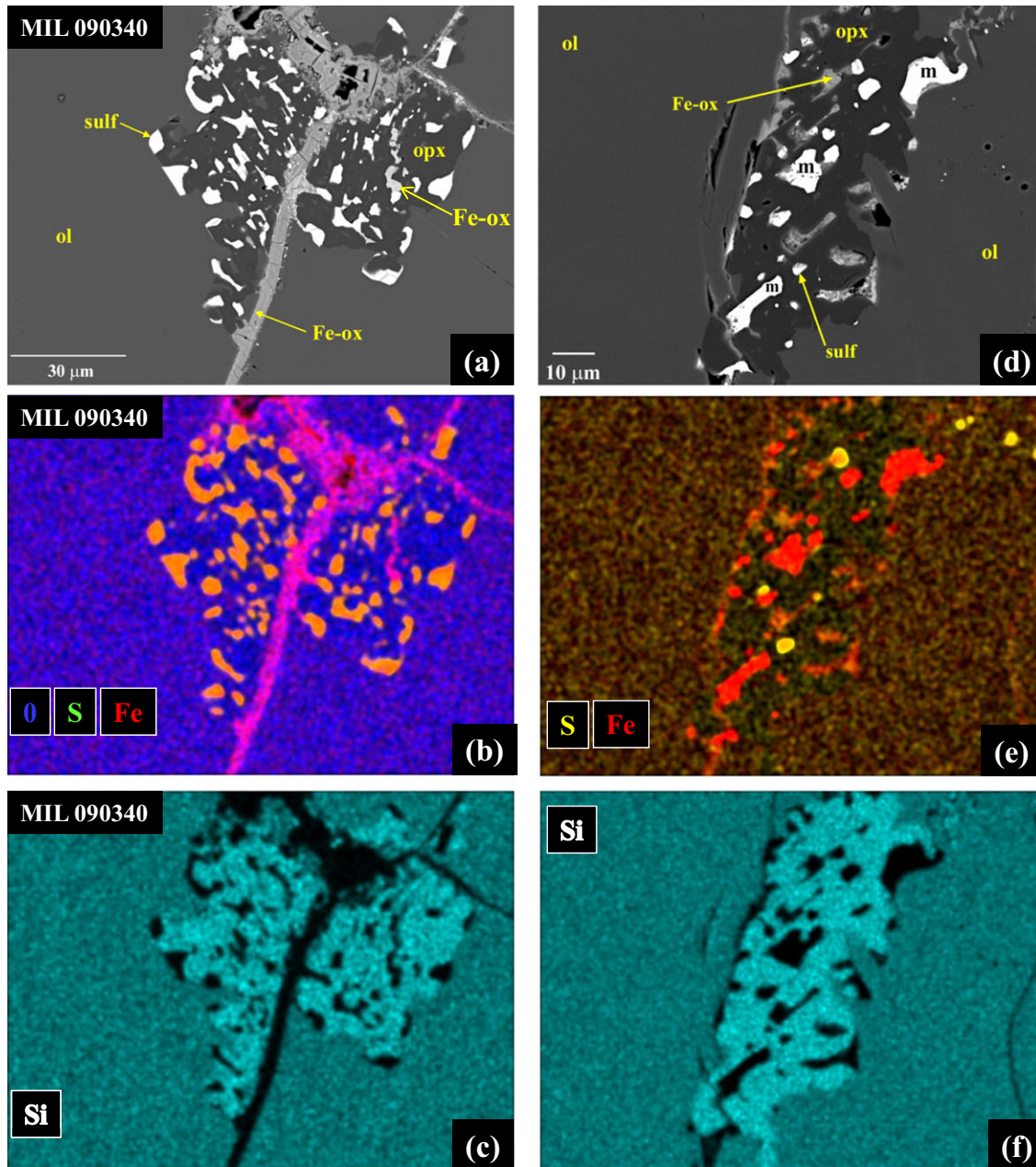


Fig. 11. Fine-grained intergrowths of orthopyroxene (opx) plus opaques along margins of olivine grains in MIL 090340. In (a–c), most of the preserved opaques (not altered to Fe-oxides) are sulfide. In (d–f), most of the preserved opaques are metal. a) BEI. b) Combined Fe (red), O (blue), and S (green) x-ray map of area in (a). c) Si X-ray map of area in (a). d) BEI. e) Combined Fe (red) and S (yellow) x-ray map of area in (d). f) Si x-ray map of area in (d). Phase labels as in Figs. 1–4.

IW-2.8 (consistent with fO_2 values previously inferred from olivine-silica-iron equilibria). Values obtained for the chromite-bearing ureilites are several orders of magnitude higher, ranging from \sim IW to IW+1.0. Applying Equation 1 to the brachinites yields inferred fO_2 values of IW+1.7 (\pm 0.5), IW+3.2 (\pm 0.5), and IW+3.1 (\pm 0.3), for Brachina, Nova 003, and Hughes 026, respectively, even higher than those of the

chromite-bearing ureilites. Likewise, MIL 090340 and MIL 090206 yield fO_2 values similar to those of the brachinites: IW+2.3 (\pm 0.5) and IW+2.2 (\pm 0.4), for MIL 090206 (nonpoikilitic) and MIL 090340, respectively. The values for the brachinites and MIL samples are one to two orders of magnitude more oxidized than the most oxidized ureilite measured to date (LAP 03587).

Table 6. Cr valence results for the olivine grains from MIL 090206 and MIL 090340 and brachinites (Brachina, Nova 003, and Hughes 026). The valences for each grain are determined from a synthetic spectrum produced by merging spectra collected at different orientations and the standard deviation values reflect the variation in the valences determined separately for each orientation (see text).

MIL 090206 (oikocryst; Fo 76.1 ± 0.6)		
	Cr valence	Std. Dev.
Grain 1	2.76	0.04
Grain 3	2.71	0.06
Mean	2.74	
Std. Dev.	0.04	
MIL 090206 (Fo 72.3 ± 0.1)		
	Cr valence	Std. Dev.
Grain 5	2.68	0.04
Grain 7	2.59	0.07
Grain 9	2.53	0.01
Grain 11	2.56	0.10
Grain 13	2.51	0.11
Grain 15	2.66	0.05
Mean	2.59	
Std. Dev.	0.07	
MIL 090340 (Fo 71.3 ± 0.6)		
	Cr valence	Std. Dev.
Grain 1	2.57	0.07
Grain 3	2.61	0.05
Grain 5	2.51	0.07
Grain 7	2.53	0.08
Grain 9	2.56	0.06
Grain 11	2.57	0.05
Grain 13	2.68	0.08
Grain 15	2.50	0.11
Mean	2.57	
Std. Dev.	0.06	
Brachina (Fo 69.5 ± 0.5)		
	Cr valence	Std. Dev.
Grain 1	2.46	0.09
Grain 2	2.62	0.05
Grain 3	2.51	0.08
Grain 4	2.46	0.06
Grain 5	2.44	0.11
Mean	2.50	
Std. Dev.	0.07	
Nova 003 (Fo 66.8)		
	Cr valence	Std. Dev.
Grain 1	2.66	0.09
Grain 2	2.69	0.05
Grain 3	2.64	0.05

Table 6. *Continued.* Cr valence results for the olivine grains from MIL 090206 and MIL 090340 and brachinites (Brachina, Nova 003, and Hughes 026). The valences for each grain are determined from a synthetic spectrum produced by merging spectra collected at different orientations and the standard deviation values reflect the variation in the valences determined separately for each orientation (see text).

Nova 003 (Fo 66.8)		
	Cr valence	Std. Dev.
Grain 4	2.78	0.04
Grain 5	2.72	0.11
Mean	2.70	
Std. Dev.	0.06	
Hughes 026 (Fo 65.9)		
	Cr valence	Std. Dev.
Grain 1	2.64	0.10
Grain 2	2.68	0.07
Grain 3	2.72	0.01
Grain 4	2.73	0.06
Grain 5	2.68	0.05
Mean	2.69	
Std. Dev.	0.04	

The fO_2 values obtained here for the MIL samples and brachinites, assuming igneous equilibration between olivine and melt at 1200 °C, are also several log units more oxidized than fO_2 inferences obtained by other approaches. Thermodynamic calculations by Gardner-Vandy et al. (2013) indicate typical brachinite fO_2 s are near IW-1 (including Hughes 026) with the exception of Brachina, which is near IW, i.e., more oxidized than typical brachinites. In contrast, the results presented here suggest Brachina is more reduced. Vanadium XANES measurements on spinels by Righter et al. (2016) yielded values near IW+0.5 for two brachinites (neither analyzed in this study), i.e., more oxidized than the Gardner-Vandy et al. results but still more reduced than the Cr results reported here.

Temperature is a potential source of systematic error in fO_2 calculations, since redox equilibria and partition coefficients are potentially temperature-dependent and estimated equilibration temperatures for the MIL samples and the brachinites are lower than the 1200 °C for which Equation 1 was determined and the 1200–1300 °C at which ureilites equilibrated. As discussed above, based on the olivine-augite thermometer, the brachinites equilibrated at ~1000 °C (again, Brachina is an exception and yields temperatures of ~1150–1200 °C), and the two MIL samples equilibrated at ~930 °C. Based on the olivine-chromite thermometer, equilibration

Table 7. Cr valence results for olivine grains from five low-Fo ureilites: LAP 02382, META 78008, HaH 064, Shisr 007, and PCA 82506.

HaH 064 (Fo 77.4)	Cr valence	Std. Dev.
Grain 1a	2.325	0.11
Grain 1b	2.29	0.07
Grain 2	2.27	0.07
Grain 3a	2.17	0.18
Grain 3b	2.17	0.17
Grain 4	2.22	0.16
Grain 5	2.21	0.18
Grain 6	2.18	0.19
Grain 8a	2.31	0.10
Grain 8b	2.30	0.12
Grain 10	2.19	0.18
Grain 11	2.32	0.13
Grain 12	2.24	0.11
Grain 13	2.3	0.13
Mean	2.25	
Std. Dev.	0.06	
LAP 02382 (Fo 78.4)	Cr valence	Std. Dev.
Grain 1a	2.24	0.18
Grain 1b	2.29	0.19
Grain 2a	2.21	0.15
Grain 2b	2.24	0.16
Grain 3	2.23	0.09
Grain 4	2.28	0.14
Grain 5	2.31	0.11
Grain 6	2.36	0.13
Grain 7a	2.30	0.15
Grain 7b	2.34	0.15
Grain 8	2.32	0.17
Grain 9	2.31	0.15
Grain 10	2.38	0.07
Grain 11	2.34	0.10
Mean	2.25	
Std. Dev.	0.04	
PCA 82506 (Fo 78.3)	Cr Valence	Std. Dev.
Grain 1a	2.16	0.07
Grain 1b	2.15	0.09
Grain 2	2.12	0.16
Grain 3	2.15	0.17
Grain 4	2.16	0.10
Grain 5	2.29	0.02
Grain 6	2.31	0.03
Grain 7	2.27	0.03
Grain 8	2.31	0.05
Mean	2.15	
Std. Dev.	0.02	
META 78008 (Fo 75.9)	Cr valence	Std. Dev.
Grain 1	2.32	0.13
Grain 2	2.28	0.14
Grain 3	2.30	0.18

Table 7. *Continued.* Cr valence results for olivine grains from five low-Fo ureilites: LAP 02382, META 78008, HaH 064, Shisr 007, and PCA 82506.

META 78008 (Fo 75.9)	Cr valence	Std. Dev.
Grain 4	2.29	0.16
Grain 5	2.23	0.15
Grain 6	2.25	0.13
Grain 7	2.32	0.12
Grain 8	2.35	0.06
Grain 9	2.31	0.16
Mean	2.28	
Std. Dev.	0.03	
Shisr 007 (Fo 79.0)	Cr valence	Std. Dev.
Grain 1	2.25	0.19
Grain 2	2.19	0.13
Grain 3	2.23	0.16
Grain 4	2.29	0.09
Grain 5	2.22	0.19
Grain 6	2.19	0.14
Grain 7	2.19	0.15
Grain 8	2.27	0.09
Grain 9	2.20	0.10
Grain 10	2.18	0.13
Mean	2.22	
Std. Dev.	0.04	

temperatures were even lower, ~895–930 °C. Below, we consider the effect of low equilibration temperature with and without the presence of melt.

In the presence of melt, there are two effects at the lower temperature compared to the assumed 1200 °C: (1) the partition coefficient $D(\text{Cr}^{2+})$ is greater (while $D[\text{Cr}^{3+}]$ is temperature independent), and (2) the melt is more oxidized. Hanson and Jones (1998) showed that, for Fe-free and Fe-bearing systems, $\ln[D(\text{Cr}^{2+})]$ exhibits a single linear trend versus $1/T$, although data only exist down to 1120 °C. Consequently, we consider two extremes, (1) the lowest temperature datum of Hanson and Jones (1998) at 1120 °C represents a plateau level, or (2) the trend can be extrapolated linearly to lower temperature. $D(\text{Cr}^{2+})$ values for 900 °C are constrained by these two extremes to be between 1.3 and 3.1. Thus, if the MIL olivine valences of ~2.6 ($\text{Cr}^{2+}/\text{Cr}^{3+} = 0.67$) were established in the presence of melt at 900 °C, the associated melt $\text{Cr}^{2+}/\text{Cr}^{3+}$ would be between 0.22 and 0.52. Unfortunately, data do not exist for “ $f\text{O}_2$ versus valence” for silicate melt at 900 °C. As an alternative, we correct the melt valence from 900 °C to 1200 °C at fixed $f\text{O}_2$ then apply Equation 1. Schreiber (1986) showed that, for a redox couple, $\log(\text{reduced species}/\text{oxidized species})$ is linear in $1/T$ with a slope proportional to the enthalpy of reduction, ΔH . The results of Schreiber and Haskin (1976) suggest a value of

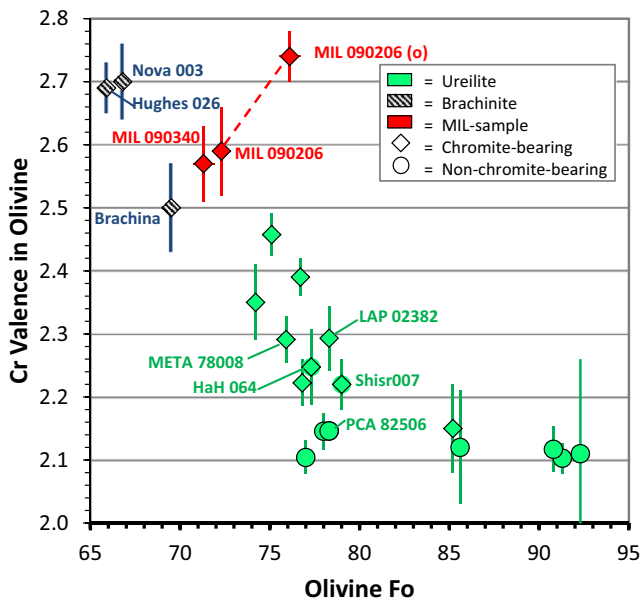


Fig. 12. Cr valence state versus Fo for olivine in MIL 090340, MIL 090206, brachinites, and ureilites. Ureilites (green symbols) include previously reported results (Goodrich et al. 2013a) and new data (indicated with labels). Brachinites shown with blue symbols and the MIL samples with red. Diamonds indicate chromite-bearing meteorites (see Goodrich et al. 2013a). Circles indicate samples in which no chromite was observed. MIL090206 has olivine in two occurrences, as grains in nonpoikilitic areas and as chadocrysts in a large orthopyroxene oikocryst. The latter are labeled “MIL090206 (o).” Results for the two occurrences are connected by a dashed line. The valence values are the mean results for the multiple grains analyzed in different orientations in each meteorite and the error bars are the standard deviations of the valences for grain suite in each meteorite. The ureilite olivines contain more reduced Cr (non-chromite-bearing olivine most reduced) than the brachinite and MIL samples. The chadocryst olivine in MIL 090206 is more oxidized (and has higher Fo) than the other, nonpoikilitic olivine in that meteorite. (Color figure can be viewed at wileyonlinelibrary.com.)

~40 kcal/mol for ΔH (FAD composition) in which case increasing the temperature of the melt from 900 °C to 1200 °C at fixed fO_2 will yield more reduced Cr by a factor of 2.3, i.e., $Cr^{2+}/Cr^{3+} = 0.51-1.20$. Using Equation 1 for 1200 °C, this redox ratio range corresponds to fO_2 range of IW+1.3 to +2.9. Thus, our fO_2 result assuming closure at 1200 °C, IW+2.3 (± 0.5), could be too oxidized by at most 1 log unit in this scenario, potentially bringing the result to within 1 log unit of the vanadium valence value from the Righter et al. (2016) study on spinel.

A more likely scenario is that melt was absent at the equilibration temperatures relevant to olivine-chromite equilibration, in which case subsolidus redox equilibration could be significant. MIL90340 is 97% olivine and 0.6% chromite with other phases being

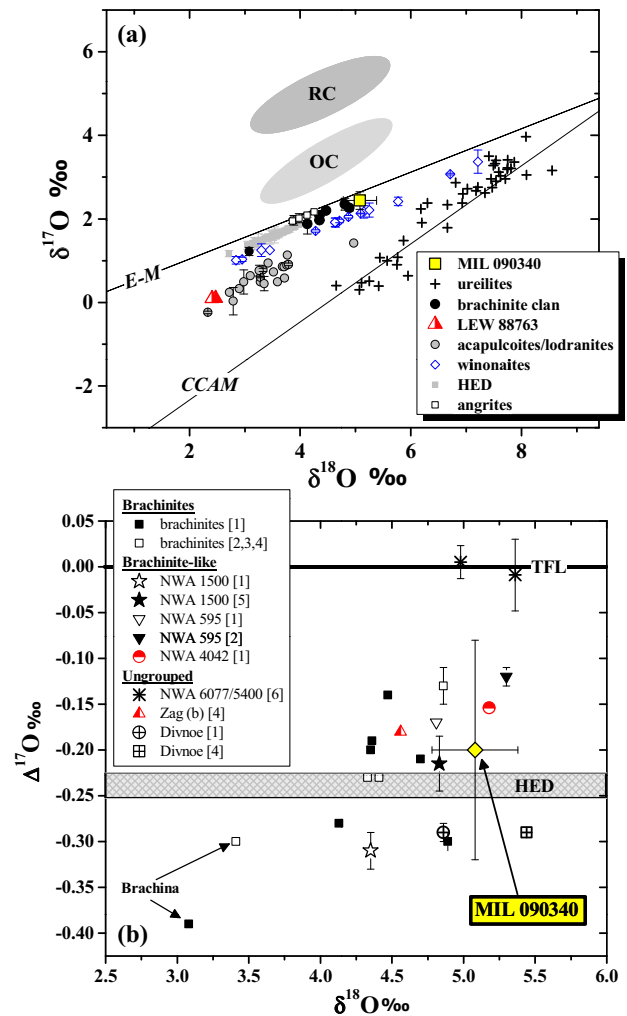


Fig. 13. a) Three oxygen isotope plot for solar system materials, showing SIMS data for olivine in MIL 090340 (this work) compared with bulk compositions of various types of achondrites. The oxygen isotope composition of olivine in MIL 090340 (which must be nearly identical to that of the whole rock because the sample consists of 97% olivine) is consistent with the brachinite trend and distinct from the ureilite trend. CCAM = carbonaceous chondrite anhydrous mixing line (Clayton and Mayeda 1999). OC = ordinary chondrite field (Clayton et al. 1991). RC = Rumuruti-type chondrite field (Bischoff et al. 2011). Achondrite data (EATG residues only) from Greenwood et al. (2005, 2012), except ureilites from Clayton and Mayeda (1996). LEW 88763 data from Greenwood et al. (2012) and Day et al. (2015). b) $\delta^{18}O$ versus $\Delta^{17}O$ for olivine in MIL 090340 compared with bulk compositions for brachinites, brachinite-like achondrites, and some ungrouped achondrites. Note that LEW 88763 and Tafassasset do not plot within the region of this diagram. MIL 090206 was reported to have $\Delta^{17}O = -0.15$, but no $\delta^{18}O$ value was given (Corder et al. 2014). [1] Greenwood et al. (2012); [2] Irving et al. (2005); [3] Irving and Rumble (2006); [4] Rumble et al. (2008). [5] Goodrich et al. (2011); [6] Day et al. (2012). All $\Delta^{17}O$ values are calculated (or recalculated from published data for $\delta^{17}O$ and $\delta^{18}O$) using the expression of Miller (2002). (Color figure can be viewed at wileyonlinelibrary.com.)

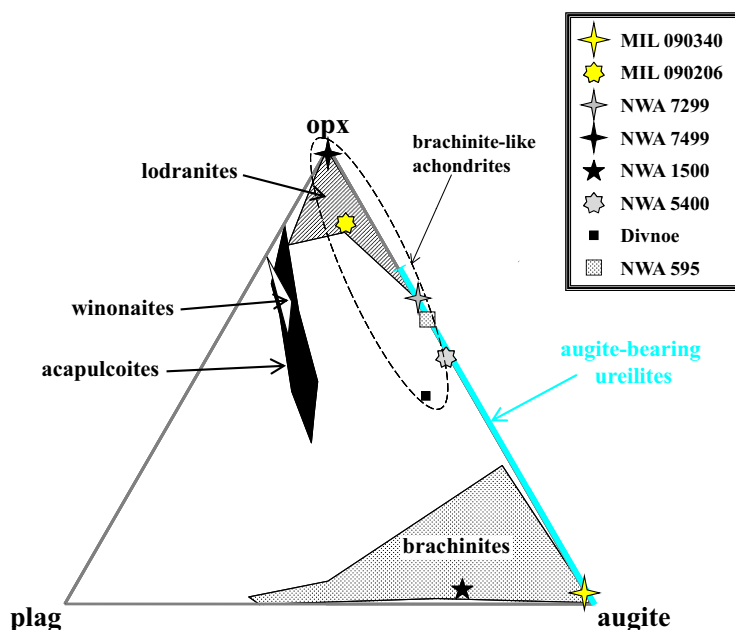


Fig. 14. Modal abundances (renormalized without olivine) of plagioclase (plag), orthopyroxene (opx), and augite in MIL 090340 and MIL 090206, compared with those in various groups of olivine-rich primitive achondrites. Sources for data fields are as given in the caption to fig. 2a of Goodrich et al. (2011). Additional data from Meteoritical Bulletin Database and Gardner-Vandy et al. (2013). (Color figure can be viewed at wileyonlinelibrary.com.)

negligible contributors to whole rock Cr. The Cr concentration in the chromite is near 40% by weight (Table 3). Olivine Cr is near detection limit by EMP (Table 1) and we use an upper limit of 500 ppm here. Thus, 83% of the Cr is hosted by chromite and 17% by olivine. The Cr valence in the former will be stoichiometrically constrained to be pure Cr^{3+} at the time of crystallization. Assuming olivine crystallized at high temperature near IW, it will have a Cr valence of ~ 2.3 (using Equation 1 and assuming unity partitioning). In a closed system, the rock will equilibrate under subsolidus conditions as it cools to the closing temperature of $\sim 900^\circ\text{C}$ striving to achieve a valence of 2.9, the weighted whole rock average. Essentially, a redox gradient exists that moves Cr^{3+} from chromite to olivine. Our measured olivine valence of 2.6 is therefore an intermediate state in this scenario requiring a doubling of the Cr^{3+} content of the olivine (30% to 60%). Since the Cr^{3+} diffusion involves less than 1% of the Cr in chromite, little effect on the chromite composition would result. A similar calculation for vanadium suggests that $>90\%$ of V is hosted by olivine. Because there are no significant crystal chemical controls on V valence, subsolidus equilibration will insignificantly alter the original V valence in these phases, thus explaining the lower $f\text{O}_2$ values obtained from V valences (Righter et al. 2016).

Subsolidus Cr valence re-equilibration between olivine and chromite is plausible, even when pyroxenes

record higher temperatures such as those given by the two-pyroxene or augite-olivine thermometers above. This is because the olivine-chromite thermometer records principally Fe/Mg equilibration, which is well known to be much more rapid in olivine than in pyroxene, and diffusion coefficients for Cr in olivine have been found to be similar to those of Fe-Mg interdiffusion (Jones and Lofgren 1993). Re-equilibration is also supported by the homogeneity of the chromite and most olivine grains. The slight reverse Fe/Mg zonation observed in a few olivine grains is associated with formation of the grain boundary assemblages, which likely occurred at lower temperatures than the Cr valence re-equilibration.

There are clearly uncertainties related to the apparent low equilibration temperatures of these rocks and details of their subsolidus histories, processes that could impact our ability to accurately infer oxygen fugacities at temperatures significantly below those of the Hanson and Jones (1998) study. Consequently, the $f\text{O}_2$ values relative to IW estimated using Equation 1 may be reasonably accurate for Brachina, but $f\text{O}_2$ results for Nova 003, Hughes 026, MIL 090206, and MIL 090340 are likely to be too oxidized as a result of subsolidus equilibration.

Classification of MIL 090340 and MIL 090206

Based on the preceding comparisons of the petrographic, mineral compositional, oxygen isotopic,

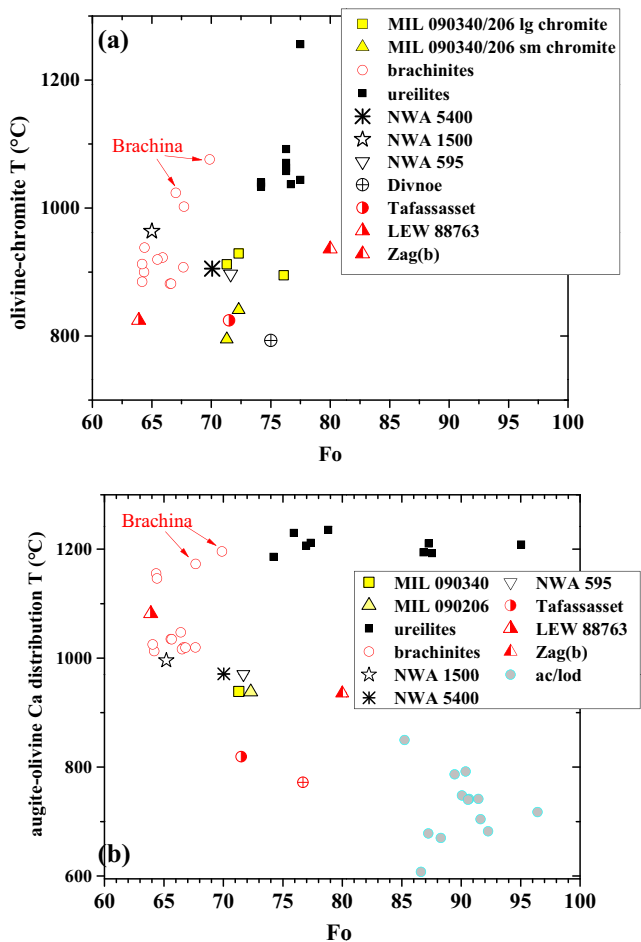


Fig. 15. a) Olivine-chromite equilibration temperatures (Wlotzka 2005) versus Fo of olivine for MIL 090340 and MIL 090206, compared with ureilites, brachinites and brachinite-like achondrites, and some ungrouped achondrites. Sources of data for calculated temperatures are the same as in Fig. 9. b) Equilibration temperatures based on the distribution of Ca between olivine and augite (Köhler and Brey 1990) for MIL 090340 and MIL 090206, compared with ureilites, brachinites and brachinite-like achondrites, acapulcoites and lodranites, and some ungrouped achondrites. Sources of data for calculated temperatures are the same as in Fig. 9, with the addition of Takeda (1989), Takeda et al. (1989, 1994), Goodrich et al. (2001, 2009), Weber et al. (2003), and this work. (Color figure can be viewed at wileyonlinelibrary.com.)

and Cr valence properties of MIL 090340 and MIL 090206 with those of various other olivine-rich achondrites, we conclude that these two meteorites are brachinite-like achondrites.

Origin of Grain Boundary Orthopyroxene + Opaques Assemblages in Brachinites and Brachinite-Like Achondrites

Intergrowths of orthopyroxene + opaques like those along olivine grain margins in MIL 090340 and MIL

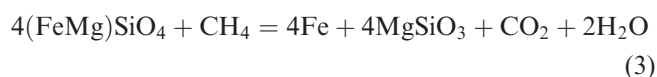
090206 have been described in brachinites or brachinite-like achondrites Reid 013, Hughes 026, NWA 1500, NWA 4872, NWA 4874, NWA 4882, NWA 4969, NWA 5191, NWA 7388, and NWA 7605 (Rumble et al. 2008; Goodrich et al. 2011; Irving et al. 2013). These intergrowths are superficially similar to the characteristic reduction rims and veins found on ureilite olivine. In particular, they lead to grain boundary darkening, which gives them a compelling resemblance to ureilites in transmitted light viewing. However, there are significant differences between these grain boundary intergrowths in brachinites and the reduction rims in ureilites.

In ureilites, reduction rims on olivine grains (typically 5–10 μm wide, though in some cases more extensive) consist of olivine that is steeply reverse-zoned from homogeneous internal grain compositions (Fo as low as 75) to more magnesian compositions (often up to Fo ~99), and which contains numerous tiny grains of Fe metal. In rare cases, magnesian orthopyroxene occurs in addition to or instead of olivine in these rims (e.g., Berkley and Jones 1982; Goodrich et al. 2013b). In most cases, the metal grains do not show any preferred orientation within these olivine rims but instead appear randomly situated. In rare cases, they appear to be dispersed in dotted lines along fracture or cleavage planes within the olivine (see fig. 1d in Goodrich et al. 2013b), but they do not show the cuneiform morphologies observed in the brachinites. Sulfide grains are sometimes found within reduction rims or veins in ureilites, but are far less abundant than metal. In rare cases, narrow reduction rims occur on pigeonite grains in ureilites, where they consist of orthopyroxene plus tiny metal grains with the metal showing no preferred orientation (see fig. 1d in Goodrich et al. 2013b). The reduction rims and veins in ureilites are commonly interpreted as a product of late reaction between olivine and graphite (reduction of olivine) located along grain boundaries or as inclusions (Wlotzka 1972; Warren 2012).

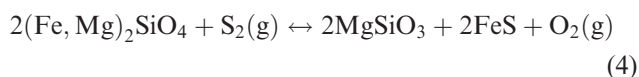
In contrast, the grain boundary intergrowths that occur in brachinites and brachinite-like achondrites occur exclusively on olivine and consist exclusively of orthopyroxene (rather than Mg-enriched olivine) plus opaques. With the exception of NWA 1500 (Goodrich et al. 2011), they do not appear to be accompanied by significant zonation in the host olivine grains. However, the slight reverse zonation of olivine that we observed in MIL 090340 and MIL 090206 suggests that other brachinites and brachinite-like achondrites should be more carefully examined to see if they show olivine zoning. Perhaps most importantly, in contrast to ureilites, the opaques in the brachinite intergrowths include a significant amount of sulfide, in addition to metal.

Determining the origin of these intergrowths in brachinites and brachinite-like achondrites depends

critically on constraining their original (preterrestrial weathering) sulfide/metal ratio. Goodrich et al. (2011) argued that although sulfide is now more abundant than metal in these intergrowths (from observations of NWA 1500, Hughes 026, Reid 013, NWA 5191, and NWA 595), metal would have been preferentially weathered and therefore the original assemblage was probably dominated by metal. Based on this assumption, Goodrich et al. (2011) reasoned that these intergrowths most likely resulted from a reduction process, but acknowledged that there was no evidence of the reducing agent or the nature of the reaction, since brachinites are not known to contain graphite or significant carbon. Irving et al. (2013) suggested that they might have formed by methane infiltration and reduction of olivine, e.g.,



However, the observations made here for MIL 090340 and MIL 090206 strongly suggest that sulfide was originally far more abundant than metal in these intergrowths (though metal was also present). Singerling et al. (2013) reached this conclusion as well, and proposed that these intergrowths in the six similar MIL meteorites (MIL 090340, MIL 090206, MIL 090356, MIL 090405, MIL 090805, MIL 090963) formed by sulfidation (sic) of primary olivine by a S-rich fluid/gas, e.g.,

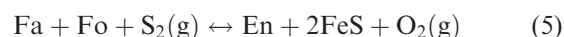


They noted, however, that this idealized reaction is too simplistic, because the orthopyroxene in the brachinite intergrowths is only slightly more magnesian than host olivine, rather than being pure enstatite.

Symplectite intergrowths of orthopyroxene + troilite have been reported in a variety of settings in various meteorites, which suggests that the process(es) than can lead to their formation is(are) not uncommon. El Goresy et al. (2005) described patches of orthopyroxene + troilite symplectites along boundaries between primary orthopyroxene and troilite grains in Acapulco, and interpreted them to result from crystallization of a sulfide-silicate partial melt. Patzer and McSween (2012) described vermicular orthopyroxene + troilite ("2-phase symplectites") in diagenetic components of several howardites, and interpreted them to result from localized, shock-induced melting of orthopyroxene and troilite grains, with subsequent quenching of the melt. Zhang et al. (2013) described fine-grained porous areas within

pyroxene and plagioclase grains in a eucrite, in which the original minerals appear to have been replaced by fine-grained intergrowths of troilite and various secondary silicates. They attribute these replacement textures to reaction with S-rich vapors. Perhaps most similar to the brachinite intergrowths, Norman (1981), Lindstrom and Salpas (1983) and Norman et al. (1995) have described replacement of olivine by troilite + enstatite in plutonic clasts in lunar fragmental breccia 67016.

Colson (1992) discussed the origin of these lunar replacement textures and proposed the general sulfurization reaction



They noted that this reaction would not be triggered by a decrease in pressure, or a decrease in temperature at constant O_2/S_2 , but could be triggered by a decrease in O_2/S_2 such as would occur if O_2 was buffered as temperature decreased. As discussed by Norman et al. (1995), although olivine reacts readily with S-bearing vapor (Kullerud and Yoder 1963, 1964; Kullerud and Yoder 1963, 1964), large proportions of S to olivine are necessary to avoid forming iron-oxides as reaction products, unless $f\text{O}_2$ is buffered (as suggested by Colson 1992). Shearer et al. (2012) explored these reactions further, taking into account the compositions of the original lunar olivine and the compositions and proportions of reaction products, and concluded that the reaction must have involved loss of Mg and that the S-rich vapor also transported chalcophile-siderophile elements.

If the brachinite grain boundary intergrowths, indeed, formed mainly as orthopyroxene + sulfide (rather than orthopyroxene + metal), then it seems likely that they originate from interaction of primary olivine with introduced S-rich vapors via reactions such as those discussed by Singerling et al. (2013), Colson (1992), Norman et al. (1995), and Shearer et al. (2012). Unfortunately, detailed analysis of the reactions involved is precluded at this time by the high degree of terrestrial weathering in all studied samples that show this intergrowth. Nevertheless, the presence of some metal in these intergrowths suggests that in some cases, or to some degree, the reactions must have also involved either reduction or mobilization of Fe, Ni metal. The pronounced reverse zonation of olivine in NWA 1500 (Goodrich et al. 2011) and the lesser reverse zonation observed in MIL 090340 and MIL 090206 in this study support this conclusion. Minor and trace element analyses of the metal and sulfide might provide further information on the reactions involved in formation of these intergrowths.

Implications of MIL 090340 and MIL 090206 for Petrogenesis of Brachinites and Brachinite-Like Achondrites

Brachinites and brachinite-like achondrites share a common Fe-Mn-Mg redox trend (Fig. 6a) that is distinct from the Fe-Mn-Mg redox trends of ureilites, lodranites/acapulcoites, or winonaites, and have higher olivine Fe/Mg ratio (lower Fo) than these other primitive achondrite groups. This observation suggests that brachinites and brachinite-like achondrites are derived from a common nebular reservoir, which had homogeneous Mn/Mg ratio and was relatively oxidized. We suggest that brachinites and brachinite-like achondrites be collectively called the brachinite clan. Nevertheless, these meteorites are diverse in petrologic features and oxygen isotope compositions (even among the brachinites alone), with no correlations between $\Delta^{17}\text{O}$ and petrologic features such as texture (granoblastic versus poikilitic), Fo of olivine, modal abundance of plagioclase or pyroxenes, or the presence of grain boundary orthopyroxene+opaques assemblages. Thus, it has been suggested that they represent more than one parent body (Rumble et al. 2008; Day et al. 2012; Greenwood et al. 2012).

MIL 090340 and MIL 090206 add to the diversity within the brachinite clan. MIL 090340 has a granoblastic texture and modal mineralogy similar to most brachinites, but a Fo value (71.3) more like those of brachinite-like achondrites. The granoblastic textured area of MIL 090206 has modal abundances, Fo (72.3), Cr valences in olivine, and cosmic ray exposure ages (Welten et al. 2014) similar to MIL 090340, but this sample also contains an extensive area of poikilitic pyroxene, as in other brachinite-like achondrites (S1). Thus, these two samples seem to blur the distinction between brachinites and brachinite-like achondrites. That is, if brachinites are defined by modal abundances and texture, then their Fo values extend to more magnesian compositions than previously thought, and/or if brachinite-like achondrites are defined by Fo values and presence of significant orthopyroxene, then they may or may not show poikilitic textures. Welten et al. (2014) concluded that MIL 090340 and MIL 090206 are paired. We suggest that even if they are not actually paired (i.e., broken off from the same meteoroid in Earth's atmosphere), they could have been derived from the same lithologic unit on a common parent body. If this is correct, the $\Delta^{17}\text{O}$ value reported by Corder et al. (2014) for MIL 090206 would also indicate that this parent body had been incompletely homogenized in oxygen isotopes during igneous processing, as discussed previously by Rumble et al. (2008), Greenwood et al. (2012), and Day et al. (2012) for brachinites and brachinite-like achondrite parent bodies in general.

A basic question of brachinite petrogenesis that has been discussed in the literature is whether these meteorites are magmatic cumulates or partial melt residues (see synopsis in Keil 2014). Most researchers (e.g., Goodrich et al. 2011; Day et al. 2012; Gardner-Vandy et al. 2013) now argue that brachinites are primitive achondrites (as originally suggested by Nehru et al. 1983, 1996)—i.e., they are residues resulting from various low degrees of melting of, and melt migration within, chondritic precursor materials. The principal petrologic evidence for this interpretation is their Fe/Mg-Fe/Mn trend (Fig. 6a), which is defined by a near-constant, approximately chondritic Mn/Mg ratio. Such trends, which are also shown by other primitive achondrite groups such as ureilites, acapulcoites/lodranites, and winonaites, are inconsistent with a relationship by igneous fractionation (which produce trends of near-constant Fe/Mn ratio over a range of Fe/Mg ratio). Instead, they suggest various degrees of oxidation/reduction of common material, with low degrees ($\leq 20\%$) of partial melting within each sample (Goodrich and Delaney 2000; Goodrich and Righter 2000; Mittlefehldt et al. 2003; Goodrich et al. 2011). Other types of evidence supporting a residue, rather than melt, origin for brachinites include heterogeneous oxygen isotope ($\Delta^{17}\text{O}$) compositions and “near-chondritic” ($\sim 2\text{--}10 \times \text{CI}$) abundances of highly siderophile elements (e.g., Day et al. 2012; Greenwood et al. 2012; Day and Warren 2015).

Nevertheless, some features of brachinites and brachinite-like achondrites do suggest a cumulate character. These include the intergranular morphologies of plagioclase and augite in many brachinites, coarse poikilitic augite in brachinite ALH 84025 (Warren and Kallemeyn 1989), and coarse poikilitic orthopyroxene and augite in brachinite-like achondrites, including MIL 090206. These features are not inconsistent with an essentially residue origin, and could be a result of limited melt migration, with trapping and subsequent recrystallization of small volumes of melt in the residual matrix. Again, the similar petrology, Cr valence, and cosmic ray exposure ages of MIL 090340 and the granoblastic part of MIL 090206 provide evidence that samples with significant “cumulate character” (MIL 090206) could be derived from the same geologic environment as samples with purely “residue character” (MIL 090340). If the poikilitic area of MIL 090206 is, indeed, a product of trapped melt, then the more magnesian compositions of the olivine chadocrysts in this area might suggest late reduction, relative to the conditions prevailing in source regions during partial melting. However, the nearly identical Fe/Mn ratios of olivine in the two areas (Fig. 6a), and the higher (more oxidized) Cr valence of olivine chadocrysts in the

poikilitic region, are not consistent with this interpretation (see Goodrich and Delaney 2000). The Fe/Mn ratio suggests instead that the olivine chadocrysts experienced a higher degree of melting than olivine in the nonpoikilitic areas, possibly due to longer duration of contact with the melts (also suggested by their small size). The higher Cr valence could reflect a lower temperature (at the same oxygen fugacity relative to IW, as discussed above) for the same reason. Such a scenario is plausible if the melt invaded and was trapped in residual material along lines of weakness and the melt fraction was small. Olivines in immediate contact with the melt would have equilibrated with it faster than the rest of the rock. This could be tested in future work by looking for possible valence (and Fo) gradients in the nonpoikilitic olivine approaching the oikocryst.

There is also no apparent correlation of $\Delta^{17}\text{O}$ or Fo with presence or absence of symplectic orthopyroxene + sulfide/metal intergrowths among brachinite clan meteorites. Thus, it is not clear whether the difference between the presence and absence of these features corresponds to different parent bodies. We note, however, that if they formed from invasion of S-rich vapors, as discussed above, then it is plausible this mechanism operated heterogeneously on the scale of an asteroid. Norman et al. (1995) and Shearer et al. (2012) suggested that the heat source for generation of S-rich vapors in the Moon was emplacement of magmas into the crust, with either the intrusions themselves being the source for the S or the S being remobilized from troilite already present in the crustal rocks. Such a source for the S-rich vapors is unlikely on a primitive achondrite parent body, which is unlikely to have experienced more than one episode of melting. A more likely heat source would be impacts. Although the brachinite clan samples that contain the orthopyroxene + sulfide/metal intergrowths are not themselves highly shocked (MIL 090340 and MIL 090206 being examples), it is conceivable that the S-rich vapors were generated by impacts elsewhere on their parent bodies and migrated into these samples.

Acknowledgments—We thank Addi Bischoff, Joseph Boesenberg, Shawn Wallace, Rainer Bartoschewitz, and the Antarctic Meteorite Working Group for the loan of samples. We thank Michael Jercinovic at the University of Massachusetts, Amherst, for assistance with SEM and EMPA work. Discussions with Paul Warren and Alan Rubin are greatly appreciated. We thank Kathryn Gardner-Vandy and James Day for helpful reviews, and Gretchen Benedix for editorial handling. This work was supported by NASA grant NNX12AH74G to Cyrena Goodrich, and by the Lunar and Planetary Institute. Portions of this work were performed at

GeoSoilEnviroCARS (Sector 13), Advanced Photon Source (APS), Argonne National Laboratory. GeoSoilEnviroCARS is supported by the National Science Foundation—Earth Sciences (EAR-1128799) and Department of Energy—GeoSciences (DE-FG02-94ER14466). This research used resources of the Advanced Photon Source, a U.S. Department of Energy (DOE) Office of Science User Facility operated for the DOE Office of Science by Argonne National Laboratory under Contract No. DE-AC02-06CH11357. XANES data analysis by Andrea Bryant was supported by the NASA RIS4E Virtual Institute (publication #SSERVI-2016-002). This paper is PSI contribution No. #634 and LPI contribution #1988.

Editorial Handling—Dr. Gretchen Benedix

REFERENCES

- Andersen D. J., Lindsley D. H., and Davidson P. M. 1993. QUILF: A PASCAL program to assess equilibria among Fe-Mg-Mn-Ti oxides, pyroxenes, olivine, and quartz. *Computers and Geoscience* 19:1333–1350.
- Antarctic Meteorite Newsletter*. 34, #1, 2011.
- Benedix G. K., Lauretta D. S., and McCoy T. J. 2005. Thermodynamic constraints on the formation conditions of winonaites and silicate-bearing IAB irons. *Geochimica et Cosmochimica Acta* 69:5123–5131.
- Berkley J. L. and Jones J. H. 1982. Primary igneous carbon in ureilites: Petrological implications. Proceedings, 13th Lunar and Planetary Science Conference, Part 1. *Journal of Geophysical Research* 87:A353–A364.
- Berry A. J. and O'Neill H. C. St. 2004. A XANES determination of the oxidation state of chromium in silicate glasses. *American Mineralogist* 89:790–797.
- Bischoff A., Vogel N., and Roszjar J. 2011. The Rumuruti chondrite group. *Chemie der Erde* 71:101–133.
- Burroni A. and Folco L. 2008. Frontier Mountain meteorite specimens of the acapulcoite-lodranite clan: Petrography, pairing, and parent-rock lithology of an unusual intrusive rock. *Meteoritics & Planetary Science* 43:731–744.
- Clayton R. N. and Mayeda T. K. 1996. Oxygen isotope studies of achondrites. *Geochimica et Cosmochimica Acta* 60:1999–2017.
- Clayton R. N. and Mayeda T. K. 1999. Oxygen isotope studies of carbonaceous chondrites. *Geochimica et Cosmochimica Acta* 63:2089–2104.
- Clayton R. N., Mayeda T. K., Goswami J. N., and Olsen E. J. 1991. Oxygen isotope studies of ordinary chondrites. *Geochimica et Cosmochimica Acta* 55:2317–2237.
- Colson R. O. 1992. Mineralization on the Moon? Theoretical considerations of Apollo 16 “rusty rocks,” sulfide replacement in 67016, and surface-correlated volatiles on lunar volcanic glass. *Proceedings of Lunar and Planetary Science* 22:427–436.
- Corder C. A., Day J. M. D., Rumble D. III, Assayag N., Cartigny P., and Taylor L. A. 2014. Petrology and geochemistry of achondrites LEW 88763, MIL 090206 and MIL 090405: Comparisons with acapulcoites-lodranites, brachinites and chondrites (abstract #2752). 45th Lunar and Planetary Science Conference. CD-ROM.

- Day J. M. D. and Warren P. H. 2015. Highly siderophile element abundance and Os isotope systematics of partially-melted FeO-rich achondrite meteorites (abstract #1254). 46th Lunar and Planetary Science Conference. CD-ROM.
- Day J. M. D., Walker R. J., Ash R. D., Liu Y., Rumble D. III, Irving A. J., Goodrich C. A., Tait K., McDonough W. F., and Taylor L. A. 2012. Origin of felsic achondrites Graves Nunataks 06128 and 06129, and ultramafic brachinites and brachinite-like achondrites by partial melting of volatile-rich primitive parent bodies. *Geochimica et Cosmochimica Acta* 81:94–128.
- Day J. M. D., Corder C. A., Rumble D. III, Assayag N., Cartigny P., and Taylor L. A. 2015. Differentiation processes in FeO-rich asteroids revealed by the achondrite Lewis Cliff 88763. *Meteoritics & Planetary Science* 50:1750–1766.
- Delaney J. S., Zanda B., Clayton R. N., and Mayeda T. 2000. Zag(b): A ferroan achondrite intermediate between brachinites and lodranites (abstract #1745). 31st Lunar and Planetary Science Conference. CD-ROM.
- Droop G. T. R. 1987. A general equation for estimating Fe³⁺ concentrations in ferromagnesian silicates and oxides from microprobe analyses, using stoichiometric criteria. *Mineralogical Magazine* 51:431–435.
- El Goresy A., Zinner E., Pellas P., and Caillet C. 2005. A menagerie of graphite morphologies in the Acapulco meteorite with diverse carbon and nitrogen isotopic signatures: Implications for the evolution history of acapulcoite meteorites. *Geochimica et Cosmochimica Acta* 69:4535–4556.
- Folco L., D'Orazio M., and Burrioni A. 2006. Frontier Mountain 93001: A coarse-grained, enstatite-augite-oligoclase-rich, igneous rock from the acapulcoite-lodranite parent asteroid. *Meteoritics & Planetary Science* 41:1183–1198.
- Gardner-Vandy K. G. 2012. Partial melting on FeO-rich asteroids: Insights to the first stage of planetary differentiation. PhD Dissertation. Tucson, Arizona: University of Arizona.
- Gardner-Vandy K. G., Lauretta D. S., Greenwood R. C., McCoy T. J., and Killgore M. 2012. The Tafassasset primitive achondrite: Insights into initial stages of planetary differentiation. *Geochimica et Cosmochimica Acta* 85:142–159.
- Gardner-Vandy K. G., Lauretta D. S., and McCoy T. J. 2013. A petrologic, thermodynamic and experimental study of brachinites: Partial melt residues of an R chondrite-like precursor. *Geochimica et Cosmochimica Acta* 122:36–57.
- Goodrich C. A. and Delaney J. S. 2000. Fe/Mg-Fe/Mn relations of meteorites and primary heterogeneity of primitive achondrite parent bodies. *Geochimica et Cosmochimica Acta* 64:2255–2273.
- Goodrich C. A. and Righter K. 2000. Petrology of unique achondrite QUE 93148. A piece of the HED mantle? *Meteoritics & Planetary Science* 35:521–535.
- Goodrich C. A., Jones J. H., and Berkley J. L. 1987. Origin and evolution of the ureilite parent magmas: Multi-stage igneous activity on a large parent body. *Geochimica et Cosmochimica Acta* 51:2255–2273.
- Goodrich C. A., Fioretti A. M., Tribaudino M., and Molin G. 2001. Primary trapped melt inclusions in olivine in the olivine-augite-orthopyroxene ureilite Hughes 009. *Geochimica et Cosmochimica Acta* 65:621–652.
- Goodrich C. A., Scott E. R. D., and Fioretti A. M. 2004. Ureilitic breccias: Clues to the petrologic structure and impact disruption of the ureilite parent body. *Chemie der Erde* 64:283–327.
- Goodrich C. A., Wlotzka F., Ross D. K., and Bartoschewitz R. 2006. Northwest Africa 1500: Plagioclase-bearing monomict ureilite or ungrouped achondrite? *Meteoritics & Planetary Science* 41:925–952.
- Goodrich C. A., Fioretti A. M., and Van Orman J. A. 2009. Petrogenesis of augite-bearing ureilites Hughes 009 and FRO 90054/93008 inferred from melt inclusions in olivine, augite and orthopyroxene. *Geochimica et Cosmochimica Acta* 73:3055–3076.
- Goodrich C. A., Kita N. T., Spicuzza M. J., Valley J. W., Zipfel J., Mikouchi T., and Miyamoto M. 2011. The Northwest Africa 1500 meteorite: Not a ureilite, maybe a brachinite. *Meteoritics & Planetary Science* 45:1906–1928.
- Goodrich C. A., Kita N. T., Warren P. H., and Rubin A. E. 2012. MIL 090340 and MIL 090206: Two more brachinite-like achondrites mis-identified as ureilites (abstract). *Meteoritics & Planetary Science* 47:5272.
- Goodrich C. A., Sutton S. R., Wirrick S., and Jercinovic M. J. 2013a. Chromium valences in ureilite olivine and implications for ureilite petrogenesis. *Geochimica et Cosmochimica Acta* 122:280–335.
- Goodrich C. A., Ash R. D., Van Orman J. A., Domanik K., and McDonough W. F. 2013b. Metallic phases and siderophile elements in main group ureilites: Implications for ureilite petrogenesis. *Geochimica et Cosmochimica Acta* 112:340–373.
- Goodrich C. A., Harlow G., Van Orman J. A., Sutton S. R., Jercinovic M. J., and Mikouchi T. 2014. Petrology of chromite in ureilites: Deconvolution of primary oxidation states and secondary reduction processes. *Geochimica et Cosmochimica Acta* 135:126–169.
- Greenwood R. C., Franchi I. A., Jambon A., and Buchanan P. C. 2005. Widespread magma oceans on asteroidal bodies in the early solar system. *Nature* 435:916–918.
- Greenwood R. C., Franchi I. A., Gibson J. M., and Benedix G. K. 2012. Oxygen isotope variation in primitive achondrites: The influence of primordial, asteroidal and terrestrial processes. *Geochimica et Cosmochimica Acta* 94:146–163.
- Hanson B. and Jones J. H. 1998. The systematic of Cr³⁺ and Cr²⁺ partitioning between olivine and liquid in the presence of spinel. *American Mineralogist* 83:669–684.
- Irving A. J. and Rumble III D. 2006. Oxygen isotopes in Brachina, SAH 99555 and Northwest Africa 1054 (abstract). *Meteoritics & Planetary Science* 41:5288.
- Irving A. J., Kuehner S. M., and Rumble III D. 2005. Brachinite NWA 3151 and (?)brachinite NWA 595 (abstract #5213). *Meteoritics & Planetary Science* 40:5213.
- Irving A. J., Kuehner S. M., and Ziegler K. 2013. Petrology and oxygen isotopic composition of brachinite-like achondrites Northwest Africa 7388 and Northwest Africa 7605, and evidence for late-stage methane-triggered reduction (abstract #2192). 44th Lunar and Planetary Science Conference. CD-ROM.
- Johnson J. E., Scrymgeour J. M., Jarosewich E., and Mason B. 1977. Brachina meteorite—A chassignite from South Australia. *Records of the South Australia Museum* 17:309–319.
- Jones R. H. and Lofgren G. E. 1993. A comparison of FeO-rich, porphyritic olivine chondrules in unequilibrated

- chondrites and experimental analogues. *Meteoritics* 28:213–221.
- Keil K. 2014. Brachinite meteorites: Partial melt residues from an FeO-rich asteroid. *Chemie der Erde* 74:311–329.
- Kimura M., Tsuchiyama A., Fukuoka T., and Iimura Y. 1992. Antarctic primitive achondrites Yamato-74025, -75300, and -75305: Their mineralogy, thermal history, and the relevance to winonaite. *Proceedings, National Institute of Polar Research Symposium on Antarctic Meteorites* 5:165–190.
- Kita N. T., Ushikubo T., Fu B., and Valley J. W. 2009. High precision SIMS oxygen isotope analysis and the effect of sample topography. *Chemical Geology* 264:43–57.
- Kita N. T., Nagahara H., Tachibana S., Tomomura S., Spicuzza M. J., Fournelle J. H., and Valley J. W. 2010. High precision SIMS oxygen three isotope study of chondrules in LL3 chondrites: Role of ambient gas during chondrule formation. *Geochimica et Cosmochimica Acta* 74:6610–6635.
- Köhler T. P. and Brey G. P. 1990. Calcium exchange between olivine and clinopyroxene calibrated as a geothermobarometer for natural peridotites from 2 to 60 kb with applications. *Geochimica et Cosmochimica Acta* 54:2375–2388.
- Krot A. H., Keil K., Scott E. R. D., Goodrich C. A., and Weisberg M. K. 2013. Classification of meteorites and their genetic relationships. In *Meteorites, comets and planets*, edited by Davis A. M. Treatise on Geochemistry, Vol. 1, Revised edition. Amsterdam: Elsevier. pp. 1–63.
- Kullerud G. and Yoder H. S. Jr. 1963. *Sulfide-silicate reactions*. Washington, D.C.: Carnegie Institution of Washington Yearbook:215–218.
- Kullerud G. and Yoder H. S. Jr. 1964. *Sulfide-silicate reactions*. Washington, D.C.: Carnegie Institution of Washington Yearbook:218–222.
- Lindsley D. H. and Andersen D. J. 1983. A two-pyroxene thermometer. Proceedings, 13th Lunar and Planetary Science Conference, Part 2. *Journal of Geophysical Research* 88:A887–A906.
- Lindstrom M. M. and Salpas P. A. 1983. Geochemical studies of feldspathic fragmental breccias and the nature of North Ray Crater ejecta. Proceedings, 13th Lunar and Planetary Science Conference, Part 2. *Journal of Geophysical Research* 88:A671–A683.
- Miller M. F. 2002. Isotopic fractionation and the quantification of ¹⁷O anomalies in the oxygen three-isotope system: An appraisal and geochemical significance. *Geochimica et Cosmochimica Acta* 66:1881–1889.
- Mittlefehldt D. W., Lindstrom M. M., Bogard D. D., Garrison D. H., and Field S. W. 1996. Acapulco- and Lodran-like achondrites: Petrology, geochemistry, chronology, and origin. *Geochimica et Cosmochimica Acta* 60:867–882.
- Mittlefehldt D. W., McCoy T. J., Goodrich C. A., and Kracher A. 1998. Non-chondritic meteorites from asteroidal bodies. In *Planetary materials*, edited by Papike J. J. Reviews in Mineralogy, vol. 36. Washington, D.C.: Mineralogical Society of America. pp. 4–1–4–195.
- Mittlefehldt D. W., Bogard D. D., Berkley J. L., and Garrison D. 2003. Brachinites: Igneous rocks from a differentiated asteroid. *Meteoritics & Planetary Science* 38:1601–1625.
- Nehru C. E., Prinz M., Delaney J. S., Dreibus G., Palme H., Spettel B., and Wänke H. 1983. Brachina: A new type of meteorite, not a chassignite. Proceedings, 14th Lunar and Planetary Science Conference *Journal of Geophysical Research* 88:B237–B244.
- Nehru C. E., Prinz M., Weisberg M. K., Ebihara M. E., Clayton R. N., and Mayeda T. K. 1996. A new brachinite and petrogenesis of the group (abstract). 27th Lunar and Planetary Science Conference. p. 943.
- Norman M. D. 1981. Petrography of feldspathic fragmental breccia 67016: Analog of terrestrial suevite? (abstract). *Lunar and Planetary Science* 12:776–777.
- Norman M. D., Keil K., Griffin W. L., and Ryan C. G. 1995. Fragments of ancient lunar crust: Petrology and geochemistry of ferroan noritic anorthosites from the Descartes region of the Moon. *Geochimica et Cosmochimica Acta* 59:831–847.
- Patzer A. and McSween H. Y. Jr. 2012. Ordinary (mesostasis) and not-so-ordinary (symplectites) late-stage assemblages in howardites. *Meteoritics & Planetary Science* 47:1475–1490.
- Petaev M. I., Barsukova L. D., Lipschutz M. E., Wang M.-S., Ariskin A. A., Clayton R. N., and Mayeda T. K. 1994. The Divnoe meteorite: Petrology, chemistry, oxygen isotopes and origin. *Meteoritics & Planetary Science* 29:182–199.
- Ravel B. and Newville M. 2005. ATHENA, ARTEMIS, HEPHAESTUS: Data analysis for X-ray absorption spectroscopy using IFEFFIT. *Journal of Synchrotron Radiat.* 12:537–541.
- Righter K., Sutton S. R., Danielson L., Pando K., and Newville M. 2016. Redox variations in the inner solar system with new constraints from vanadium XANES in spinels. *American Mineralogist* 101:1928–1942.
- Rumble III D., Irving A. J., Bunch T. E., Wittke J. H., and Kuehner S. M. 2008. Oxygen isotopic and petrological diversity among brachinites NWA 4872, NWA 4874, NWA 4882 and NWA 4969: How many ancient parent bodies? (abstract #1974). 39th Lunar and Planetary Science Conference. CD-ROM.
- Schreiber H. D. 1986. Redox processes in glass-forming melts. *Journal of Non-Crystalline Solids* 84:129–141.
- Schreiber H. D. and Haskin L. A. 1976. Chromium in basalts: Experimental determination of redox states and partitioning among silicate phases. Proceedings, 7th Lunar Science Conference. pp. 513–538.
- Shearer C. K., Burger P. V., Guan Y., Papike J. J., Sutton S. R., and Atudorei N.-V. 2012. Origin of sulfide replacement textures in lunar breccias. Implications for vapor element transport in the lunar crust. *Geochimica et Cosmochimica Acta* 83:138–158.
- Singerling S. A., McCoy T. J., and Gardner-Vandy K. G. 2013. Possible evidence for sulfidization reactions in the Miller Range brachinites(?) (abstract #1669). 44th Lunar and Planetary Science Conference. CD-ROM.
- Sutton S. R., Bertsch P. M., Newville M., Rivers M., Lanzirrotti A., and Eng P. 2002. Microfluorescence and microtomography analyses of heterogeneous earth and environmental materials. *Reviews in Mineralogy & Geochemistry: Applications of Synchrotron Radiation in Low-Temperature & Environmental Science, Mineralogical Society of America* 49:429–483.
- Takeda H. 1989. Mineralogy of coexisting pyroxenes in magnesian ureilites and their formation conditions. *Earth and Planetary Science Letters* 93:181–194.
- Takeda H., Mori H., and Ogata H. 1989. Mineralogy of augite-bearing ureilites and the origin of their chemical trends. *Meteoritics* 24:73–81.
- Takeda H., Mori H., Hiroi T., and Saito J. 1994. Mineralogy of new Antarctic achondrites with affinity to Lodran and a

- model of their evolution in an asteroid. *Meteoritics* 29:830–842.
- Warren P. H. 2012. Parent body depth-pressure-temperature relationships and the style of the ureilite anatexis. *Meteoritics & Planetary Science* 47:209–227.
- Warren P. H. and Kallemeyn G. W. 1989. Allan Hills 84025: The second brachinite, far more differentiated than Brachina, and an ultramafic achondritic clast from L chondrite Yamato 75097. Proceedings, 19th Lunar and Planetary Science Conference. pp. 475–486.
- Warren P. H. and Rubin A. E. 2012. The Miller Range 090340 dunitite: Not a uniquely ferroan ureilite, not even a ureilite (abstract #2528). 43rd Lunar and Planetary Science Conference. CD-ROM.
- Weber I., Bischoff A., and Weber D. 2003. TEM investigations on the monomict ureilites Jalanash and Hammadah al Hamra 064. *Meteoritics & Planetary Science* 38:145–156.
- Welten K. C., Nishiizumi K., and Caffee M. W. 2014. Cosmic ray exposure history and pairing of the Miller Range ungrouped achondrites: MIL 090206, 090340 and 090963 (abstract #2450). 45th Lunar and Planetary Science Conference. CD-ROM.
- Wlotzka F. 1972. Haverö ureilite: Evidence for recrystallization and partial reduction. *Meteoritics* 7:591–600.
- Wlotzka F. 2005. Cr-spinel and chromite as petrogenetic indicators in ordinary chondrites: Equilibration temperatures of petrologic types 3.7 to 6. *Meteoritics & Planetary Science* 40:1673–1702.
- Zhang A.-C., Wang R.-C., Hsu W.-B., and Bartoschewitz R. 2013. Record of S-rich vapors on asteroid 4 Vesta: Sulfurization in the Northwest Africa 2339 eucrite. *Geochimica et Cosmochimica Acta* 109:1–13.

SUPPORTING INFORMATION

Additional supporting information may be found in the online version of this article:

Table S1: Brachinites, brachinite-like achondrites and ungrouped Olivine-rich achondrites with some similarities to brachinites

Table S2: Comparison of chromite analyses done at U. Mass with those done at AMNH

Table S3: SIMS oxygen three isotope analyses of olivine standard (Fo89 and Fo60; *1).

Table S4: SIMS oxygen three isotope analyses of olivine in MIL 09430 and San Carlos

olivine (SCOL) standard in a thin section (SC-PTS).

Fig. S1: MIL090340 – backscattered electron micrograph mosaic of the thin section showing the locations of the eight olivine grains analyzed for Cr valence.

Fig. S2: MIL090206 – backscattered electron micrograph mosaics of the thin section (full section in [a], rectangular area is magnified in [b]) showing the locations of the nineteen olivine and two opx grains analyzed for Cr valence. Grains in [b] plus grain 1 in [a] are chadocrysts within a large orthopyroxene (opx) oikocryst.